STUDY OF FLEXOELECTRIC EFFECT
IN OXIDE MATERIALS

JIN YANGSHI

MPhil

The Hong Kong Polytechnic University

2022

THE HONG KONG POLYTECHNIC UNIVERSITY

DEPARTMENT OF APPLIED PHYSICS

STUDY OF FLEXOELECTRIC EFFECT
IN OXIDE MATERIALS

JIN YANGSHI

A thesis submitted in partial fulfillment

of the requirements for the degree of Master of Philosophy

August 2021

Certificate of Originality

I hereby declare that this thesis is my own work and that, to the best of my knowledge and belief, it reproduces no material previously published or written, nor material that has been accepted for the award of any other degree or diploma, except where due acknowledgment has been made in the text.

Abstract

Flexoelectricity describes a material's electrical polarization in response to a strain gradient. Recent studies have expanded the intrinsic flexoelectric effects to a new modulation strategy in a wide range of functional materials, making the enhanced flexoelectricity a great potential for application as flexible electronics. The nature of flexoelectricity eliminates the restrictions, like the Curie temperature in many piezoelectric materials, and allows the existence and coupling with other physical properties in all materials from insulator to semiconductor as well as conductor. The coupling between flexoelectricity and photovoltaics (PV), as one of the most promising phenomena from the application point of view, has triggered many investigations and discussions in the flexoelectric community. However, there still lacks a clear physical picture to describe the flexo-photovoltaic effect, where the interactions between photon, charge, and polarization make the mechanism more complicated.

In this work, the photo-flexoelectric (photoflexoelectric) effect in perovskite structured $SrTiO_3$ (STO) single crystal was demonstrated and the coupling mechanism between its photovoltaic and flexoelectric effect was revealed. Driven by the flexoelectric field, incident light-induced electrons can tunnel through the Schottky junction at the Au/STO interface, giving rise to enhanced flexoelectricity, i.e., photoflexoelectric effect. Thermal annealing in vacuum induces oxygen vacancies in STO and results in stronger light absorption and enlarged photoflexoelectric effect. These results help us to understand the mechanism of flexoelectricity and the photoflexoelectric effect and may provide hints

of more correlation effects between flexoelectricity and photon-charge interaction. The increased flexoelectric coefficient may also have application prospects like energy harvesters and sensors.

The doping effect has also been studied in TiO_2 crystals. It is found that by introducing hydrogen dopants in TiO_2, the effective flexoelectric coefficient can be enhanced by more than two orders of magnitude compared to the pristine sample. A hydrogen charging technique has been achieved, and hydrogen doping in TiO_2 has been obtained. The mechanism of influence on the flexoelectricity by hydrogen doping in TiO_2 single crystal is attributed to the potentially formed polarization by crystal symmetry breaking due to the existence of H ions in the crystal lattice. These results broaden the horizon of study on the flexoelectricity effect in dielectric materials.

The results of this thesis demonstrate some new approaches and techniques to enhance both the intrinsic and extrinsic flexoelectricity of STO and TiO_2 crystals. These methods could be extended to different materials and find potential applications in flexible electronic devices. The physics and mechanism behind also deserve further studies.

List of Publications

1. Fan Zhang, Wei-Min Jiang, Cheng-Jian Li, <u>Yangshi Jin</u>, Zelong Wang, Jia-Cai Nie, and Ji-yan Dai, ACS Applied Electronic Materials **2** (7), 1861 (2020).

2. <u>Yangshi Jin</u>, Fan Zhang, Kai Zhou, Chun Hung Suen, XY Zhou, and Ji-Yan Dai, Applied Physics Letters **118** (16), 164101 (2021).

Acknowledgments

First and foremost, I would like to express my sincere gratitude to my supervisor, Professor Jiyan Dai, for his guidance, encouragement, and supervision. He introduced me to the field of flexoelectricity. I am thankful for his patience and perseverance in teaching me the intricacies of being a good researcher. No matter how busy he is, Professor Dai keeps standing in a forward position of material science and even come to our lab and help me in some specific experiments. His passion for research is the model for me to learn and follow in my future career. Professor Dai is always so benign and approachable. Every time I met problems in my study, Professor Dai will always spare his time in discussions with me. His suggestions are pertinent and insightful. Although spending most of his time in teaching and research, Professor Dai keeps a healthy lifestyle with frequent physical exercise. For many times, he strengthens that a strong and healthy body is the most basic requirement of research work. The things I learned from Professor Dai will influence my future career and life positively and deeply.

I should especially thank my co-supervisor Prof. SF Yu. When I encounter difficulties, he always relieves my depressed mood. When I need help, he will provide opportunities and help. He is not only my academic teacher but also a friend in life. I am very grateful to him for his help and caring during my two years of academic life

I would like to thank Prof. Shu Ping Lau, Prof. Jianhua Hao, Prof. Chi Wah Leung, Dr. Yang Chai, Dr. Xuming Zhang, and Prof. Huang Haitao for their assistance with my research and coursework studies.

I cannot neglect my senior fellow apprentice, Dr. Fan (Frank) Zhang, for his helpful advice, who professionally trained me from basics experiment skills to flexoelectricity and photovoltaic effect measurement. Dr. Zhang is not only a senior but also a close friend of mine who is always helping me in research.

None of my accomplishments would have been possible without the help and support of my colleagues. I would like to add sincere thanks to Kevin and You Huiling. They lent me experimental equipment and taught me experimental methods. Without them, I can't conduct experiments on my own.

Finally, I want to thank my friends: Wang Ting, Song Linfeng, Li Yin, Huang Ziru, and Lv Sijia due for their company during my most difficult time. Thank you to my parents Mr. Jin Wenping and Mrs. Tu Suihong very much!

Table of Contents

List of Figures

Figure 2.2 The setup of flexoelectric coefficient measurement. The cantilever bending method was used to measure the effective transverse flexoelectric coefficient. The information is collected by a lock-in amplifier.

Figure 2.3 The setup of flexoelectric coefficient measurement for U and N bending. The cantilever bending method was used to measure the effective transverse flexoelectric coefficient.

Figure 2.4. Schematic illustration of the oscillatory bending to measure direct current under zero voltage. A piezoelectric actuator is used to bend in an oscillatory manner the cantilever-shaped STO capacitor with transparent electrodes in the dark or under ultralight.

Figure 2.5 The setup of photocurrent measurement to test the photovoltaic effect. The data due to the photovoltaic effect is collected by KEITHLEY 2400 source meter.

Figure 2.6 Perovskite oxide ABO_3 structure illustration. Single cubic cell with black Sr ions at the corners, a dark gray Ti ion at the center of the cube, and light grey O ions at the centers of every faces.

Figure 2.7 The centrosymmetric oxide TiO_2 structure illustration, the blue spheres are labeled Ti, and the smaller red spheres are labeled O.

Figure 2.8 Experimental set-up for hydrogen charging. In 0.01M NaOH solution, Pt as anode and sample as cathode form an electric loop under 4.5 voltage.

Figure 3.1 Optical transmission spectra of pristine (a) and annealed (b) STO crystal with Au electrode at top and bottom surfaces.

Figure 3.2 Enhanced effective flexoelectric effect under UV light incident from the top surface of sample: (a) pristine STO under n bending, inset: the photo of the as-received pristine STO crystal, (b) pristine under u bending, (c) annealed STO sample under n bending, inset: the photo of the annealed STO crystal, and (d) annealed STO sample under u bending.

Figure 3.3 XPS spectrum of annealed STO at 700 °C for 2hrs in vacuum showing the degradation of Ti valence states from 4^+ to 3^+.

Figure 3.4 Sheet carrier density and mobility at different temperatures for the annealed STO sample.

Figure 3.5 Light-intensity dependence of flexoelectric current under a constant strain and increased UV light incident from top of the sample surface: (a) pristine STO under n bending, (b) pristine under u bending, (c) annealed STO sample under n bending, (d) annealed STO sample under u bending. The fitting curves are with the power law.

Figure 3.6 Strain gradient dependence of flexoelectric current under a constant light intensity and increased strain gradient. The notation 2,4,6,8,10 represent the amplitude of driving voltage of the vibrator which correspond to strains of 0.5, 1.0, 1.5, 2.0, and 2.5 /m, respectively.

Figure 3.7 Photocurrent of pristine and annealed STO samples. The annealed sample shows an enhanced and reversed photovoltaic effect.

Figure 4.4 *Energy band diagrams and electron tunneling at the Au/TiO$_2$ interface for pristine (a) and hydrogen-charged (b) TiO$_2$ samples. CB, energy pf conduction band minimum; VB, energy pf valence band maximum; E_ϕ, vacuum energy.*

Figure 4.5 *Effective flexoelectric effect of pristine and annealed TiO$_2$. There is no significant difference in flexoelectric coefficients between pristine TiO$_2$ and annealed TiO$_2$,* but the sign is reversed.

Figure 4.6 *the scheme of hydrogen-doped Modified model.*

Table 4.1 Modified model

Chapter I

Introduction and Literature Review

1.1 Introduction and motivation of the research

Flexoelectricity describes a material's electrical polarization in response to a strain gradient. This effect was thought to be negligible for a long time due to its much smaller magnitude compared to other electromechanical effects such as piezoelectricity. However, the emergence of flexible electronic devices, such as the bendable mobile phone, makes the study of flexible materials and related physics very attractive and timely urgent. For flexible electronic devices, the material can be subjected to a large strain gradient and induce a phenomenon called the flexoelectric effect.

Many recent studies have largely expanded the flexoelectric effects from a simple polarization concept to a new modulation strategy in a wide range of functional materials,[3,4] therefore, opening a new area of flexible electronics.[5] The idea of utilizing flexo-polarization to tailor material's physical properties is attracting more attention because of a key fact: flexoelectricity is generated from a strain gradient and is naturally accompanied by the symmetry breaking of the lattice.[6,7] This fact eliminates the restrictions, like the Curie temperature in many piezoelectric materials, and allows the existence and coupling

with other physical properties in all materials from insulator to semiconductor as well as conductor.

The flexoelectric effect is a more common phenomenon than ferroelectric and piezoelectric effects which exist only in asymmetric crystal structures. Flexoelectricity describes the generation of electric polarization under mechanical strain gradient which can break crystal space inversion symmetry, while piezoelectricity refers to the generation of electric polarization from lattice deformations in non-centrosymmetric crystals. As shown in Fig. 1.1, the principle of flexoelectric is that uneven strain causes the material crystal lattice symmetry breaking, which in turn produces polarization[6,8,9,10,11]. Since flexoelectricity is present in all-dielectric materials and is not affected by Curie temperature, its application prospects are greatly expanded.
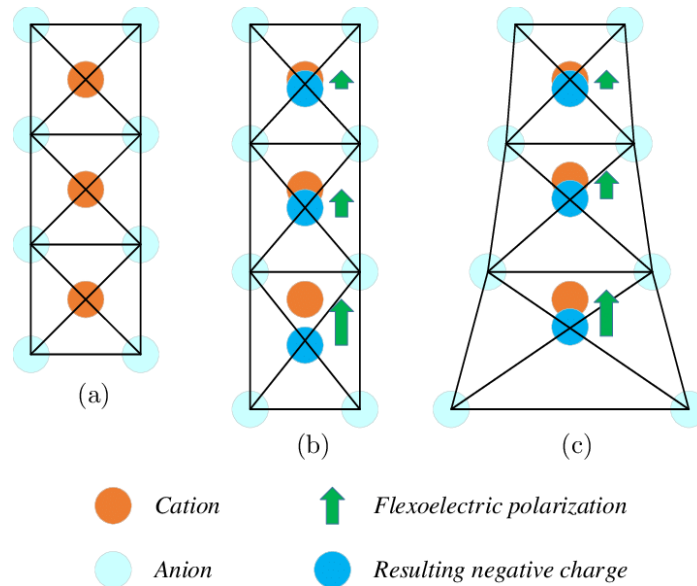
Figure 1.1 Origin of flexoelectric effect in solids. (a) Two-dimensional (2D) structure of elementary charges without dipole moment. (b) Under uniformly tensile strain for each unit cell, the tension

gradually varies from one cell to another. (c) Under inhomogeneous deformation, a dipole moment via the flexoelectric effect was induced within the unit cell.[12]

However, the physics behind the flexoelectric effect is yet to be fully understood, especially when this effect is coupled with other effects such as piezoelectricity, electrostatic charges, or in a complex structure such as thin-film heterostructures. In addition, in recent years, this topic has begun to receive more attention due to the enhancement of flexoelectricity in some thin films and specially designed structures which give rise to potential applications in electronic devices.

Due to the presence of flexoelectricity, when the material is deformed under inhomogeneous strain, the strain gradient can be equivalent to an applied electric field. With this equivalent electric field, the physical properties of the material can change greatly, giving us more room for the imagination of the coupled effect of flexoelectric with other effects such as ferroelectricity, ferromagnetism, and even flex-photovoltaics. For example, the flexoelectric field can be utilized as a modulation method to optimize the performance of conventional solar cells and photodetectors.

Nevertheless, there are also many issues and arguments in this field. For example, recently, a report in *Science* showed that uneven deformation can stimulate the photovoltaic effect in centrosymmetric materials such as $SrTiO_3$ (STO)[13]. However, the results produced by AFM tips pressure are arguable, since the tip and sample surface interaction may result in a very complicated situation that is far different from their expectations[14]. Therefore, it

is desired to demonstrate these modulations such as flexo-photovoltaics in a bulk sample through a macroscopic approach.

Centrosymmetric materials such as $SrTiO_3$ and TiO_2 are very good templates for the study of coupling between flexoelectricity and other factors such as light and doping since their flexoelectric coefficients are relatively quite large among metal oxides and their crystal structures are relatively easy to analyze. As shown in Fig. 1.2, to enhance the flexoelectricity in some dielectrics, possible mechanisms have been proposed to be coupled into the flexoelectric effect, e.g., polar nanoregions, residual ferroelectricity, and surface piezoelectricity.[15,16] Zhang *et al.*[17] provided a suggestion that 70% of the increased flexoelectricity in $BaTiO_3$ perovskites is due to the surface piezoelectricity.
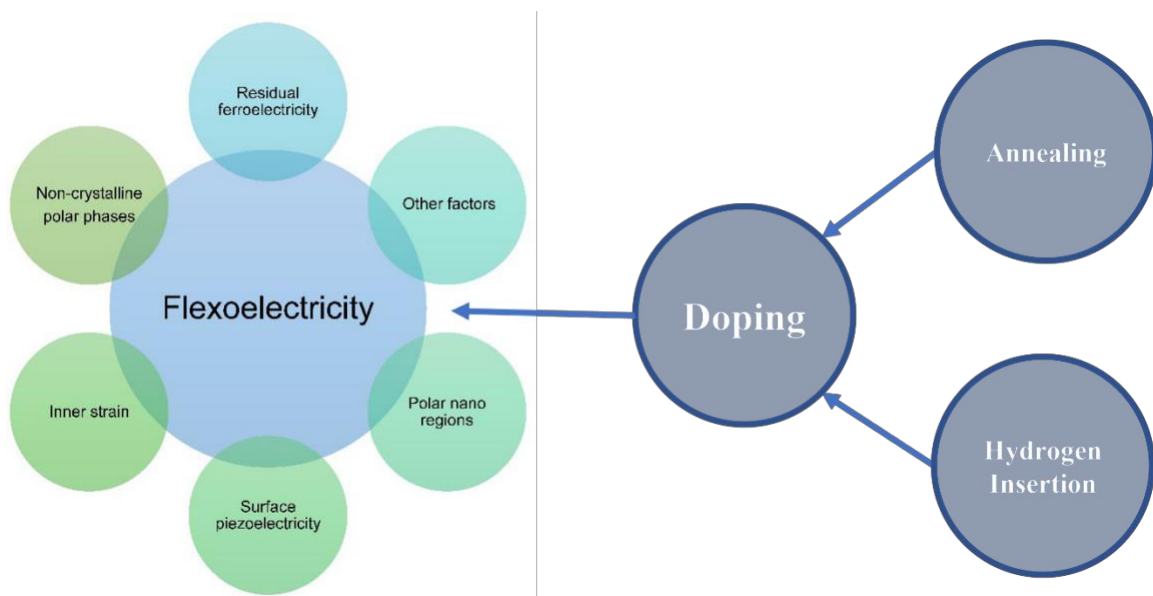
Figure 1.2 Possible mechanisms of enhanced flexoelectricity in dielectrics. In this thesis work, I propose to study enhanced flexoelectricity by light and doping.

In this thesis, their flexoelectric coefficients and the response to incident UV light for pristine and high-temperature annealed STO single crystals are studied, and coupling between the flexoelectric polarization, photo-induced current, and oxygen vacancy induced defects are revealed. To introduce dopants in bulk materials, the techniques of vacuum annealing (oxygen vacancy doping) and hydrolysis of water (hydrogen ions doping) are chosen to increase the density of charge carriers and possible electric polarization in the crystals. The findings in this work can help us to understand the mechanism of flexoelectricity and photo-flexoelectric effect and may extend present solar cell technologies by enhancing the solar energy conversion efficiency from a wide pool of established semiconductors[5]. The increased flexoelectric coefficient may also have application prospects like energy harvesters,[18] light sensors,[19] and accelerometers.[20,21]

1.2 Literature review

According to different conduction modes under applied electric field, materials are generally divided into three classes: conductors, semiconductors, and insulators. Recently, a common physical phenomenon, flexoelectricity, has attracted a lot of research interest in insulators due to its potential applications in many fields such as memory, sensors, domain engineering, actuators, defect tailoring, energy harvesters, and nanoelectronics[6,22,23,24]. The flexoelectricity refers to the contribution of the linear proportionality between the strain gradient and the electric polarization, which can be written as:

$$P_i = \mu_{ijkl} \cdot \frac{\partial \varepsilon_{kl}}{\partial x_j} \tag{1.1}$$

where P_i is the flexoelectric polarization component, ε_{kl} is the strain component, and μ_{ijkl} is the flexoelectric coefficient. The breaking of the lattice centrosymmetry contributes to the flexoelectricity, where the centers of net positive and negative charges move to opposite directions under a mechanical strain. Figure 1.3 shows a schematic demonstration of the flexoelectric effect under mechanical strain gradient.
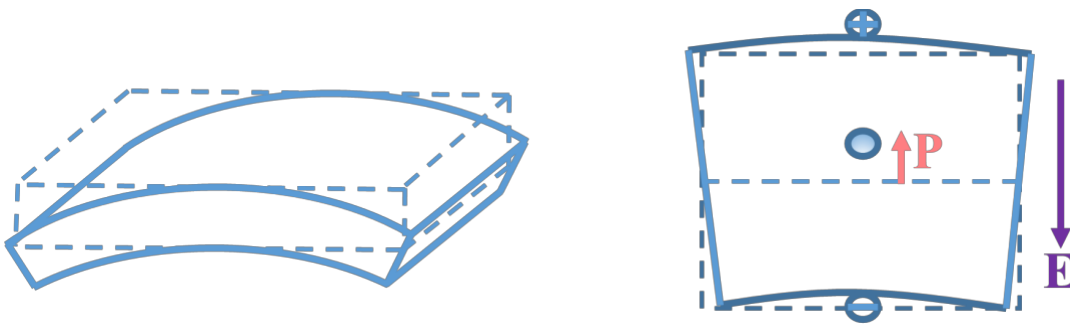
Figure 1.3 Schematic demonstration of flexoelectric effect under mechanical strain gradient, where P represents flexoelectric induced polarization and E represents the internal field induced by surface charges generated from flexoelectric effect.

In the most general case, a polarization can result from both flexoelectric and piezoelectric effects, i.e.:

$$P_i = \mu_{ijkl} \frac{\partial \varepsilon_{jk}}{\partial x_l}(flexo.) + d_{ijk}\sigma_{jk}(piezo.) \tag{1.2}$$

In this equation, P_i is the polarization vector; σ_{jk} is the second-order strain tensor; d_{ijk} is the third-order piezoelectric material property tensor; and μ_{ijkl} is the component of the flexoelectric tensor. As illustrated in Fig. 1.4, when a uniform strain is applied, electric polarization is generated from a non-centrosymmetric piezoelectric material. However, under an applied non-uniform strain, even centrosymmetric crystals locally induce charges. Different from piezoelectricity, flexoelectricity may be an all-inclusive property allowed in any structure, and thus broadens the choice of materials that can be utilized for electromechanical sensors and actuators.
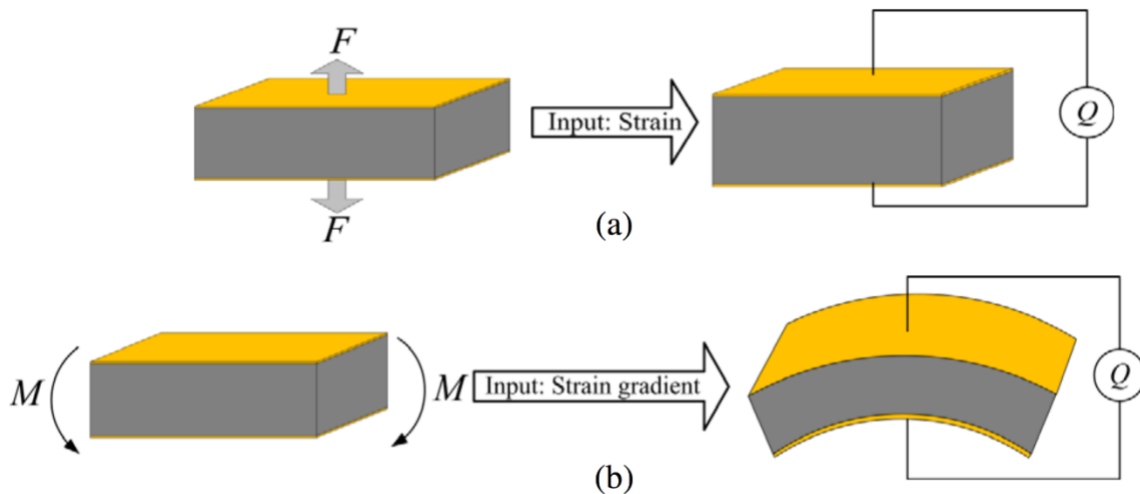
Figure 1.4 (a) piezoelectricity due to strain, and (b) flexoelectricity due to strain gradient[25]

If the polarization at the surface of the plate changes continuously from its bulk value P to zero outside the plate, the polarization gradients at the plate surfaces should create some stress via the converse flexoelectric effect, resulting in forces applied to the

opposite surfaces of the plate.[11] The Bursian-Trunov's approach treats the total free energy of the plate, implicitly considering the surface effects, where the forces are applied to the surfaces.[25] Eliseev *et al*. considered a similar bending effect that a bending-mode flexoelectric sensor working as an actuator will be characterized by the same effective piezoelectric constant. [26] For more general boundary conditions, the situation is more complex and requires the use of modified mechanical boundary conditions[12,13]. Indenbom *et al*. [27] and Eliseev *et al*. [13] derived modified boundary conditions for the polarization.

When an inhomogeneous strain or stress is induced in a perovskite material, a flexoelectric polarization field can be generated due to the flexoelectric effect[28,29,30,31]. This field not only presents on the material surface but also distributes inside the crystal over a range of lengths or volumes owing to the enormous non-uniform local strain. The inner-crystal polarization field has a huge impact on the concentration and distribution of free carriers at the metal-semiconductor interface as well as inside the semiconductor, causing band-structure engineering of both the metal-semiconductor interface and the inner crystal. In general, the negative flexoelectric polarization potential induced at the semiconductor side can repel electrons while attracting holes near the interface, enabling the energy band to be bent upward. Thus, strain-gradient-induced flexoelectric polarization can effectively modulate the interface Schottky barrier height and width, thereby controlling the charge transport, in a manner analogous to the *piezotronics* effect[32,33,34,35]. The magnitude and polarity of the flexoelectric potential depend on that of the applied inhomogeneous stress or strain. This is the flexo-electronic effect (also been called *flexotronics*), which is universal and persistent as well as exists widely in most semiconductors. The use of the

inner crystal flexoelectric polarization potential as a 'gate' controlling signal to modulate the barrier profile and achieve a tunable electronic process is the basis of flexo-electronics.

Flexoelectricity as a strain gradient-driven breaking of the local centrosymmetry can also be visualized at the microscopic level. For a simple perovskite structure, a vertical gradient of induced in-plane strain can result in the central cation being squeezed up, breaking the local centrosymmetry and inducing polarity. This analogy, based purely on steric considerations, is critical but close to the idea given by Bursian & Zaikovskii[36] that the central ion in the perovskite STO must shift down on bending or, vice versa, that bending must appear due to the shift of the Ti ion. The strain gradient in a shock wave makes unequal distances between the atomic planes, causing a local breaking of centrosymmetry. The above examples are all simple perovskite structures, with rigid ions shifting and polarization.

In 2011, Catalan found a large strain gradient in the in-plane and out-of-plane directions due to lattice mismatch between the twin domains of the $PbTiO_3$ epitaxial film. They demonstrated that the flexoelectric polarization strength caused by this strain gradient is equivalent to the ferroelectric polarization of the film, and the superposition of the two polarizations can cause the change of the domain polarization in the direction and magnitude.[23]

In 2018, Gao et al. of Peking University conducted atomic-scale measurement of the strain gradient and polarization of the misaligned center in the STO crystal by aberration-corrected scanning and transmission electron microscopy, from which atomic-scale experimental evidence of the flexoelectric effect was established.[37] As shown in Fig.

1.5, near the center of the misalignment of a 10º small-angle tilting grain boundary in the STO crystal at room temperature, they directly observed the stable electric dipole induced by the flexoelectric effect, which lead to the distortion of the oxygen octahedron near the center of the misalignment.
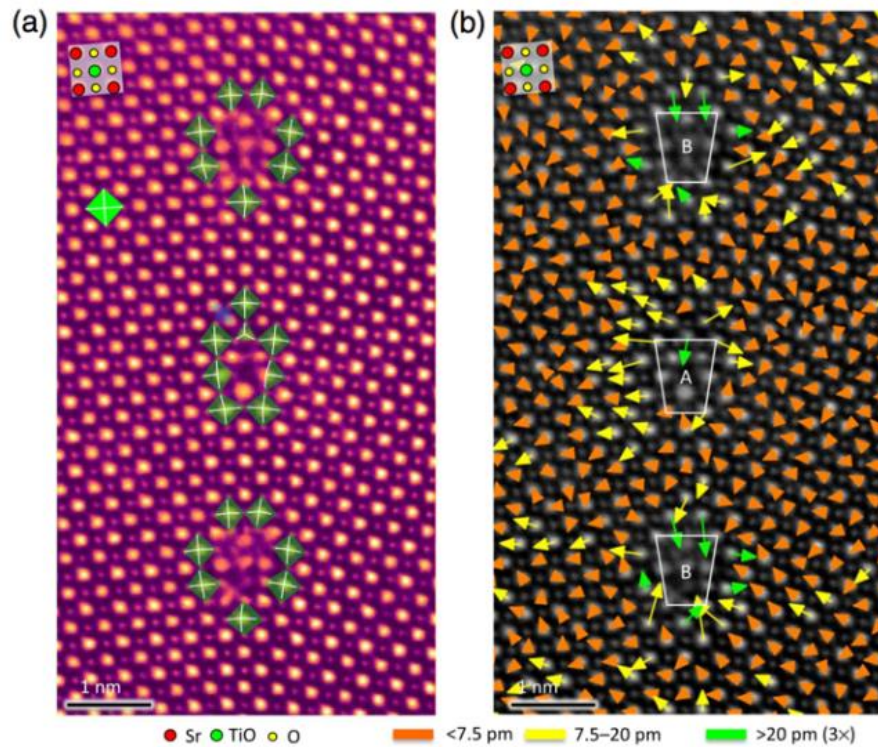
Figure 1.5 Microscopic image of strain gradient and polarization of the center of the misalignment in the STO crystal [41].

Nevertheless, an in-depth understanding of the physical mechanisms of enhancement of thin-film flexoelectricity is still not well addressed. One reason is that the traditional thin films we studied are mainly on a certain substrate, therefore, the interfacial

structure and substrate contribution to the flexoelectric effect are coupled together. The other reason is that those oxide thin films on a fragile substrate can only induce very little strain gradient. These make the study of oxide thin film flexoelectric effect quite difficult.

Besides the above-mentioned oxide crystals, the flexoelectric effect is also proven to play a crucial role in biological functions like the auditory systems[38] and bone repairing and remodeling process[39]. Very recently, theoretical work even shows that the charge separation in triboelectric effect could be driven by a flexoelectric potential difference at the nanoscale asperities[40]. All these highly inspiring results not only reveal the ubiquity of the flexoelectric phenomenon but also suggest that further investigation of flexoelectricity can help scientists understand more physical phenomena and stimulate more applications.

For thin-film electronic devices, the interfacial structure between the film and the substrate may also cause an abnormal increase in flexoelectricity. In 2011, T.W. Noh at Seoul National University and J.F. Scott of the Cambridge University jointly reported an epitaxial strain relaxation induced giant flexoelectric effects in $HoMnO_3$ (HMO) films (Fig. 1.6). Compared with conventional bulk materials, the flexoelectricity of this thin-film material has an enhancement of six orders of magnitude[44]. However, an in-depth understanding of the physical mechanisms of enhancement of thin-film flexoelectricity is still not well addressed.
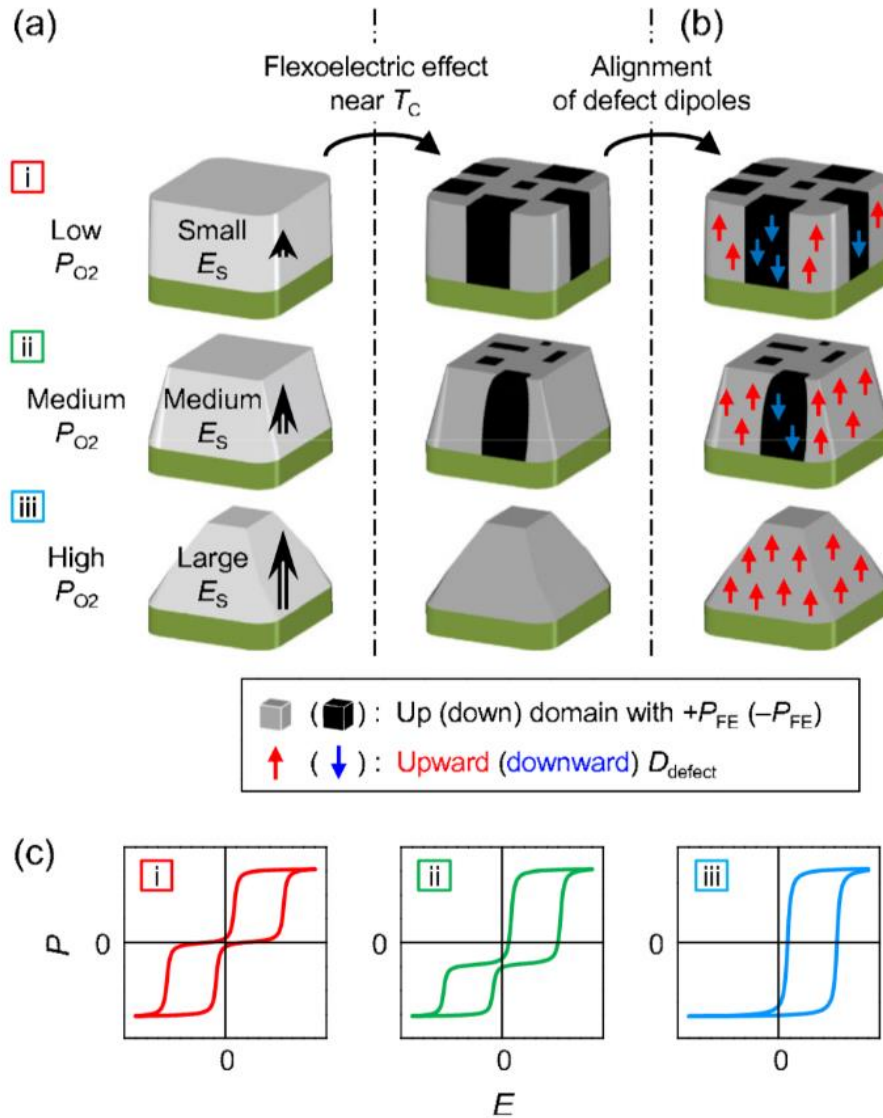
Figure 1.6 Schematic diagram showing a P_{O2} controlled epitaxial strain relaxation and its influence on the domain configurations and hysteresis curves through a giant flexoelectric effect[2].

For sensor application of flexoelectric effect, sensitivity is a key parameter. The sensitivity (S) for acoustic sensors, for example, cochlea, can be calculated by the equation

S =V/P (voltage/sound pressure)[41],[42],[43]. Recently, freestanding perovskite oxides have emerged as candidates for very large flexoelectricity due to their extremely large strain gradient. It is expected that the acoustic sensor based on the freestanding perovskite oxide films should have a much broader bandwidth and higher sensitivity than the commercial acoustic sensors based on PVDF ferroelectric polymer which has a sensitivity of about 50 mV/Pa.

The important functions of the cochlea are not only the conversion of the acoustic wave to electrical signals but also the frequency selectivity[44],[45]. Therefore, the acoustic sensor should realize both the frequency selectivity and the conversion of the acoustic wave to the electrical signal through either flexoelectric or piezoelectric or their combined effect with freestanding oxide perovskite.

Figure 1.7 shows a designed acoustic sensor and the setup of the testing system which has been used by other research groups[46] [47]. The freestanding film will be coated with Au electrode on both sides and a few micrometer-thick parylene as supporting layer (before being removed from the substrate, the film should be coated with Au electrode and parylene; and after dissolving the scarified layer, the film can be transferred to a flexible substrate such as PMA and then the other side should be coated with the patterned electrode). Parylene is a conformal protective polymer coating material utilized to uniformly protect and support the freestanding layer, and such device is highly flexible. The wedge shape of the chamber and the difference in gap widths make this device workable in liquid or air (the chamber can be filled with water). The resonance frequencies

corresponding to different gap widths at the electrode area can be calculated based on finite element simulations.
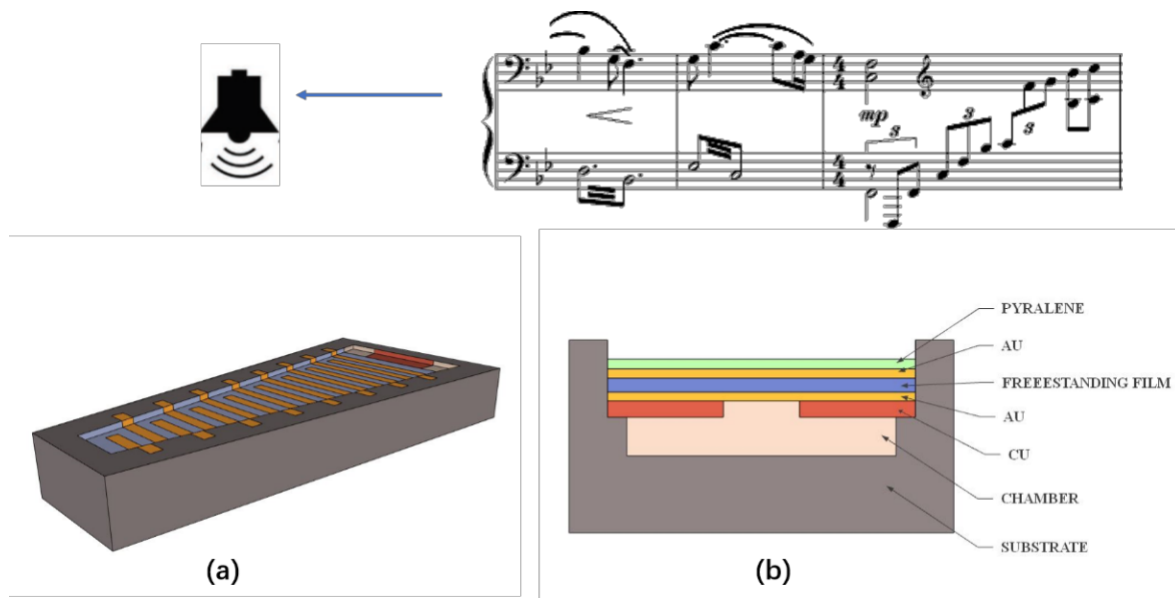
Figure 1.7 (a) Schematic diagram of the acoustic sensor device and testing setup. and (b) a cross-sectional structure of the device. The electrical signal detected between the bottom and top electrodes will be magnified by the amplifier and displayed on a digital oscilloscope. Through FFT analysis, the frequency of the read signal and input signal from the loudspeaker can be compared.

Some possible applications where flexoelectricity could be involved are developed. Wang and Wang[48] suggested an analytical model for a vibration-based circular energy harvester consisting of a flexoelectric layer and a substrate layer. Zhang et al.[49] have described a curved flexoelectric actuator by using non-polarized PVDF. A BST-based

flexoelectric curvature sensor is suggested by Yan et al.[50] Sarlo[51] has proposed an airflow sensor with artificial hair cell, as shown in Fig. 1.7.
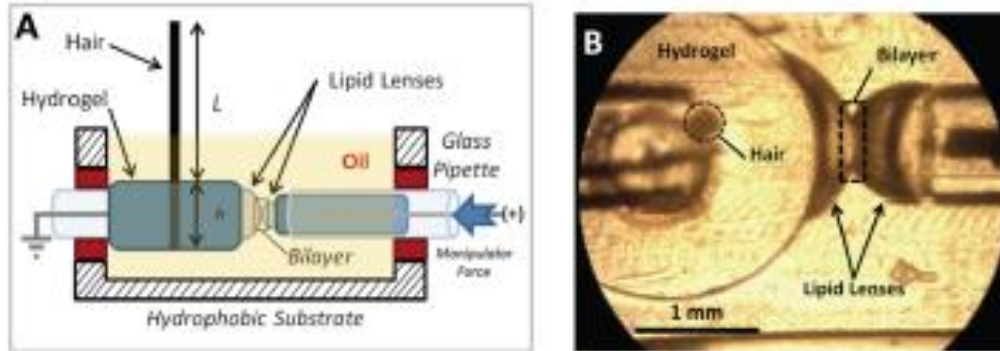
Figure 1.7 Airflow sensor with artificial hair cell.

1.3 Scope of the thesis

This thesis is divided into 5 chapters. The basic information about the flexoelectricity and photovoltaic effect is introduced in this chapter.

In Chapter II, the involved experimental techniques and setup will be illustrated. From the electrode deposition to the physical property measurement of the sample, technical parameters and the basics characterization results will be reported. The methods used to add strain to samples will be introduced.

In Chapter III, oxygen vacancy and photoelectron enhanced flexoelectricity in perovskite $SrTiO_3$ crystal will be introduced. The coupling of the photovoltaic effect and flexoelectric effect will be described to understand the enhanced flexoelectricity.

In Chapter IV, hydrogen doping enhanced flexoelectricity in rutile TiO_2 crystal will be introduced. The principle under the coupling of flexoelectricity and hydrogen incorporation will be explained.

In Chapter V, conclusions of the thesis, suggestions for future research works are given.

Chapter II

Methodology

In this chapter, the general methods to characterize the flexoelectricity and photocurrent under UV light as well as their coupling effect are introduced. Sample preparing methods including high-temperature thermal annealing and hydrogen doping into single crystal oxides materials as well as electrode deposition are also introduced.

2.1 Setup for flexoelectricity measurement

For flexoelectricity measurement, a piezoelectric actuator is utilized to deliver an oscillatory force to the free end of clamped cantilever-shaped crystals beam with a capacitor structure. The oscillatory bending induces an alternating current that is measured with a lock-in amplifier connected to the electrodes with coaxial cable metal wires. The flexoelectricity measurement setup including the clamping system is shown in Fig. 2.1, where one can see that the STO single crystal is clamped rigidly on one side and bent by a piezoelectric actuator controlled by an electronic control system with feedback displacement measurement. For a photo-flexoelectric setup, a UV light source is directly laid on the top of the cantilever.

To measure the alternating current under illumination, we used transparent electrodes based on ITO or semitransparent Au electrodes. A scheme of the experimental concept is shown in Fig. 2.1. The effective flexoelectric coefficients for STO are of the order of ~1 nC/m for both Au and transparent electrodes.

A transverse strain gradient is induced by bending the bulk crystal dynamically with a cantilever beam geometry, as shown in Fig. 2.1. A lock-in amplifier is used to collect the displacement current flowing between the upper and lower metallic electrodes to calculate the flexoelectric polarization. Polymers and perovskite oxides can be studied in this beam bending method extensively. Unlike piezoelectricity, the polarization due to flexoelectricity in dielectrics is very small but sensitive. It still has the potential to be applied in the sensor area. Flexoelectric-like response enhancement in oxide semiconductors renders the flexoelectricity new attention.
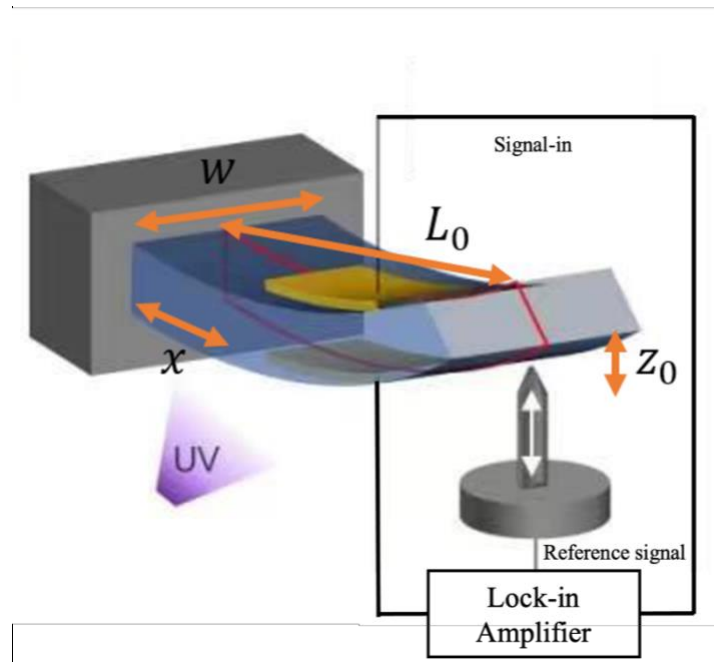
Figure 2.1 The schematic view of the bending fixtures used to introduce dynamic strain gradient to the samples illuminated by 365nm UV light. P represents flexoelectricity induced polarization from negative to positive values due to bending type.

Flexoelectricity as a strain gradient-driven breaking of the local centrosymmetry can also be visualized at the microscopic level. For a simple perovskite structure, a vertical gradient of induced in-plane strain can result in the central cation being squeezed up, breaking the local centrosymmetry, and inducing polarity. This analogy, based purely on steric considerations, is critical but close to the idea given by Bursian & Zaikovskii[52] that the central ion in the perovskite STO must shift down on bending or, vice versa, that bending must appear due to the shift of Ti ion. The strain gradient in a shock wave makes unequal distances between the atomic planes, causing a local breaking of centrosymmetry.

To measure flexoelectricity, a piezoelectric actuator is used to deliver an oscillatory force to the free end of clamped cantilever-shaped crystals, and the alternating current induced by the oscillatory bending is measured with a lock-in amplifier connected to the electrodes with coaxial cables. Using standard elastic deformation equations, for a point-loaded single-clamped beam, the strain gradient is calculated from the deflection amplitude and the distance from the clamped side and actuator contact point, and the polarization is extracted from the amplitude of the oscillating current and the frequency of the actuator. The linear proportionality constant between polarization and strain gradient is the flexoelectric coefficient.
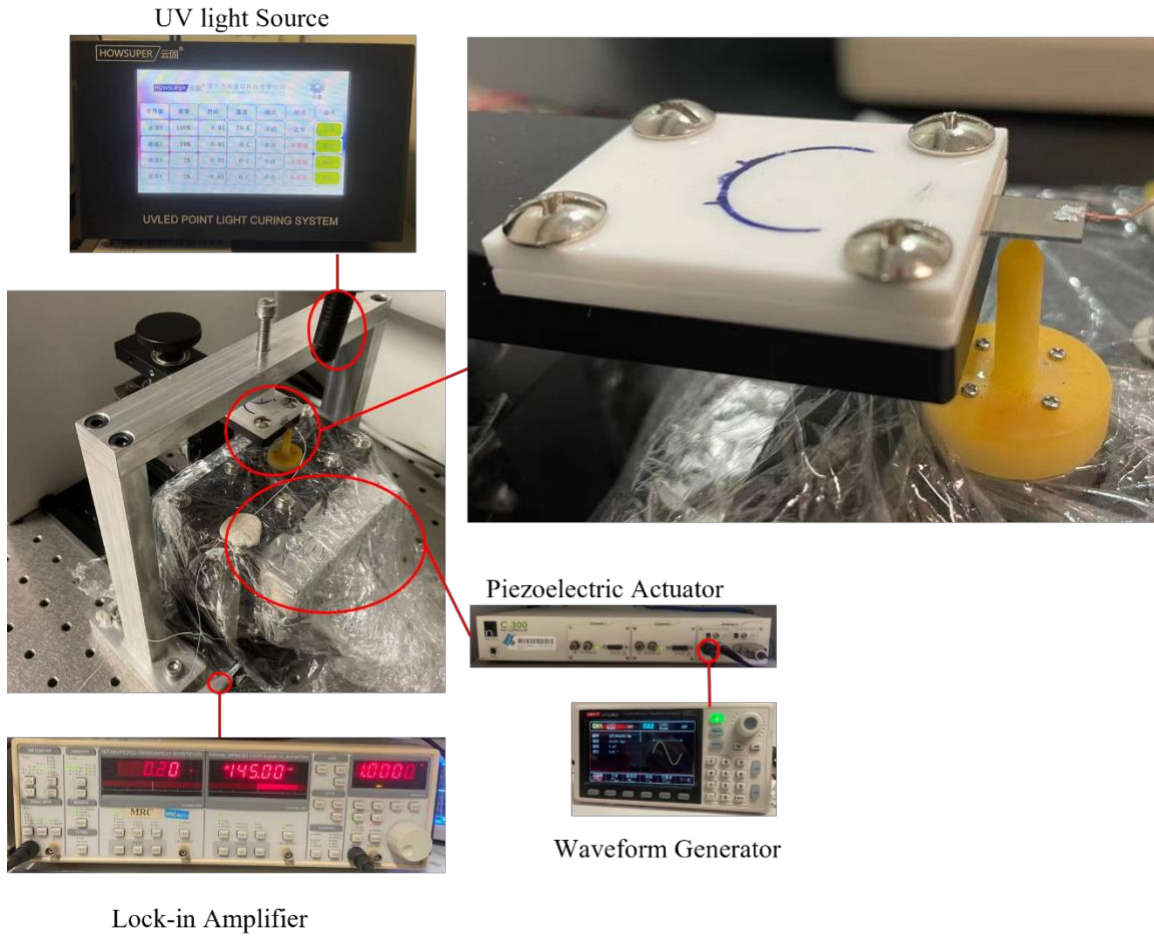
Figure 2.2 The setup of flexoelectric coefficient measurement. The cantilever bending method was used to measure the effective transverse flexoelectric coefficient. The current induced by the flexoelectric effect is collected by a lock-in amplifier.

To realize both N-type and U-type bending, we design a □ shaped sample camping tool as shown in Fig. 2.3. By clamping a sample by two sides, three-point bending

(corresponding to N bending) can be realized; while by clamping the sample at one side only, a two-point U shape bending can be realized.

Figure 2.3 The setup of flexoelectric coefficient measurement for U and N bending. The cantilever bending method is used to measure the effective transverse flexoelectric coefficient.

2.2 Flexoelectric coefficient

To calculate the flexoelectric coefficient of crystals, a lock-in amplifier (Stanford Research SR830 DSP) is used to measure flexoelectricity generated current, which is converted into charging densities P by dividing the measured current by the driving frequency and the electrode area:

$$P = \frac{I}{\omega A} \qquad (2.1)$$

where A is the area of the electrodes and $\omega = 2\pi v$ is the angular frequency of the mechanical oscillation. An oscilloscope is used for real-time monitoring of the generated signals. A signal generator provides an a.c. voltage for the actuator with a fixed frequency of 127 Hz.

The strain gradient is calculated from the elastic equation for the vertical deformation Z_0 of a point-loaded, single-clamp cantilever. The deformation can be considered quasi-static because the bending frequency (127Hz) is several orders of magnitude below the resonance frequency range of the cantilevers (tens of kHz). The clamped beam deformation is as follows:

$$y(x) = \frac{\partial x^2}{\partial L^3}(3L - x) \qquad (2.2)$$

where Z_0 is the vertical deflection delivered by the piezoelectric actuator at the end of the cantilever, L_0 is the length of the cantilever, and x is the horizontal position along the cantilever with the origin at the clamping point. The strain gradient is the curvature of the

deflection function, which is the second derivative concerning x. the average curvature under the electrode is, therefore:

$$\frac{\partial \varepsilon}{\partial x} = 3\frac{z_0}{L_0}(L_0 - x) = \frac{3}{2}\frac{z_0}{L_0^2} \tag{2.3}$$

The polarization is calculated from the current using equation (2.1), and the effective flexoelectric coefficient is defined as the induced polarization divided by the average strain gradient:

$$u = \frac{2\sqrt{2}IL_0}{3\pi f Z_0 \omega} \tag{2.4}$$

2.3 Photovoltaic effect measurement

Flexoelectricity is a property that converts mechanical energy from inhomogeneous bending into electrical energy. Nowadays, because intrinsic flexoelectric coefficients of dielectric materials of any symmetry seem to be small, it is required to achieve larger deformations so that substantial flexoelectricity can be achieved. However, the discovery of the photo-flexoelectric effect in bulk dielectric crystals has altered this landscape, i.e. increasing flexoelectricity at the macroscale by combing flexoelectricity with the photovoltaic effect.

Based on the controversial reports about the photo-flexoelectric effect and our preliminary study on bulk materials, fundamentally this photo-flexoelectric remains to be an issue. The current results may only reveal the interfacial effect at the STO/electrode.

The photocurrent should enhance the intrinsic flexoelectric effect. To measure the photocurrent, the same setup as flexoelectricity measurement was used, and the DC induced by UV light was measured with a KEITHLEY 2400 source meter.

To measure photoelectricity, a piezoelectric actuator is applied to deliver an oscillatory force to the free end of clamped cantilever-shaped crystals with a capacitor structure. The oscillatory bending induces a current which is measured with a 2400 source meter connected to the electrodes with wires (Fig. 2.4). The upward side is defined as compression while the downside is defined as tension according to the strain state on each side.
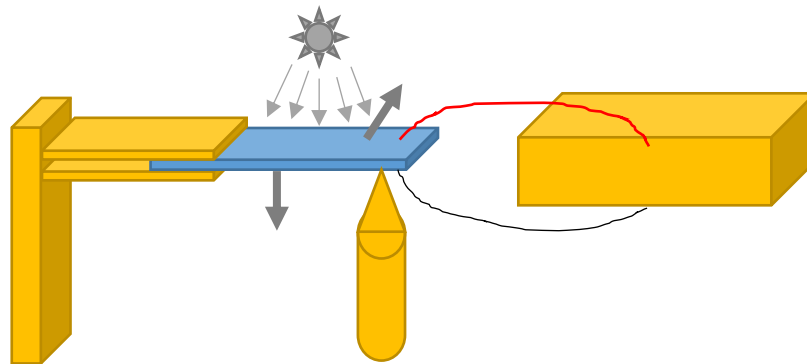
Figure 2.4 Schematic illustration of the oscillatory bending to measure direct current under zero voltage. A piezoelectric actuator is used to bend the cantilever-shaped STO capacitor in an oscillatory manner with transparent electrodes in the dark or under ultralight.

UV light Source

Piezoelectric Actuator

Waveform Generator

KEITHLEY 2400 source meter

Figure 2.5 The setup of photocurrent measurement to test the photovoltaic effect. The data due to the photovoltaic effect is collected by KEITHLEY 2400 source meter.

2.4 Samples Preparation

2.4.1 SrTiO$_3$ samples

Among the family of perovskite, strontium titanate (STO) presents particularly a wide range of physical properties and draws more attention. In addition, STO is as well classified as a band insulator with a bandgap energy of 3.2 eV. At room temperature, stoichiometric cubic STO is a centrosymmetric paraelectric material with a lattice constant of a = 3.905 Å, as illustrated in Fig. 2.4. If material is centrosymmetric to start with, it will proceed to be centrosymmetric under homogeneous deformation. STO crystal which has the common ABO$_3$ structure is a cubic perovskite where every Sr is surrounded by twelve oxygen atoms and every Ti is surrounded by six oxygen atoms. Sr sites are located at the corners, and the Ti sites are the cell center with oxygen octahedral surrounded. The Sr atom is surrounded by 8 corner-sharing TiO$_6$ octahedrons, and in some situations, it can be described as the alternatively stacking layers of SrO and TiO$_2$ along the [001] direction. That is the reason why STO is selected as a material to verify that their origin excludes ferroelectric or piezoelectric effect.
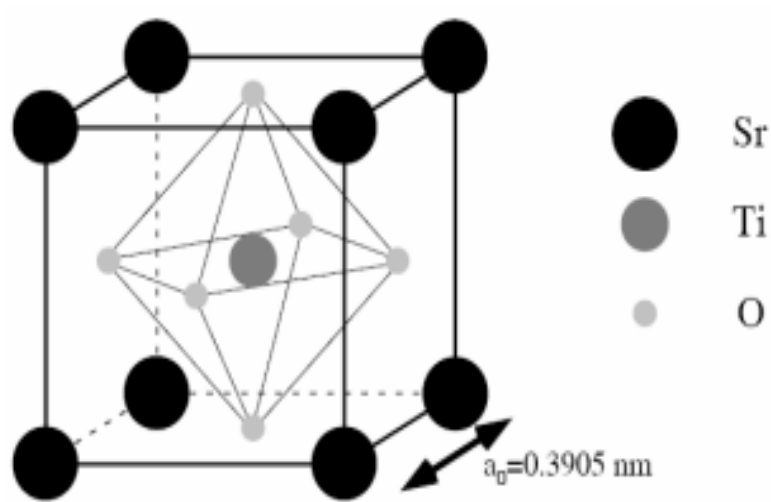
Figure 2.6 Perovskite oxide ABO₃ structure illustration. Single cubic cell with black Sr ions at the corners, a dark gray Ti ion at the center of the cube, and light grey O ions at the centers of every faces.

The STO perovskite single crystals were commercially produced by the Hefei Crystal Technical Material Co., Ltd. The orientation for STO crystals is (100) and all miscuts are required to be smaller than 0.5º. Additionally, the size of samples is 10x5x0.5 mm^3 and both surfaces are polished.

2.4.2 Rutile titanium dioxide

Titanium dioxide has three crystalline types, i.e. rutile, brookite, and anatase. Usually, the crystal structure of rutile is described in terms of the ion model based on Ti^{4+} cations and O^{2-} anions. As shown in Fig. 2.7, the red oxygen sites are arranged in the form of distorted octahedra. The structure of a rutile unit cell is tetragonal. Baur[53] has reported a=4.594 Å, c=2.959Å, and c/a=0.6441.
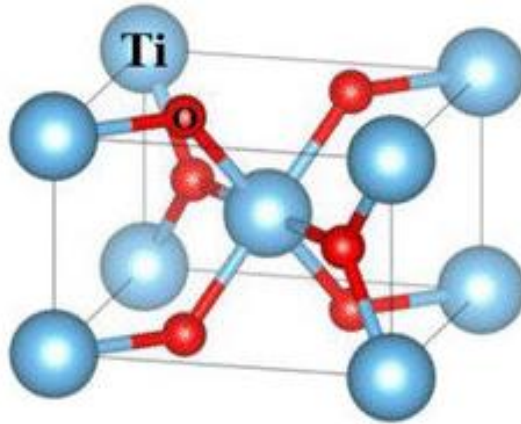
Figure 2.7 The centrosymmetry oxide TiO₂ structure illustration, the blue spheres are labeled Ti, and the smaller red spheres are O.

2.5 Hydrogen charging

To study hydrogen doping induced effect to the enhancement of flexoelectricity, rutile structured TiO_2 single crystal was selected, and the doping of hydrogen is through electrolysis water splitting. The TiO_2 sample was placed in a 0.01M NaOH water solution at 25ºC and a dc voltage was applied between the silver-coated TiO_2 sample and a Pt counter electrode in the solution, as shown in Fig.2.8. The silver electrode on the TiO_2 crystal (coated by silver past) acts as the cathode and the counter electrode acted as the anode. The crystal was then connected to the negative electrode of a 4.5 V dc voltage while the counter electrode was connected to the positive side. Electrolysis of water thus occurred due to the applied dc voltages and hydrogen gas was generated on the surface of the crystals while oxygen was evolved on the counter electrode. During this process, H^+ ions can diffusion into the TiO_2 crystal through a diffusion process driven by the electric field. This treatment is referred to as "hydrogen charging" hereafter. In this thesis, the TiO_2 single crystals were treated for 168 hours. The dc voltage was removed after the treatment and the crystals were taken out, cleaned, and dried. To study the effects of hydrogen charging in flexoelectricity, the TiO_2 single-crystal before hydrogen charging (hereafter called the "control sample") and after hydrogen charging (hereafter called the "H-doped sample") were subjected to flexoelectric coefficient measurements.
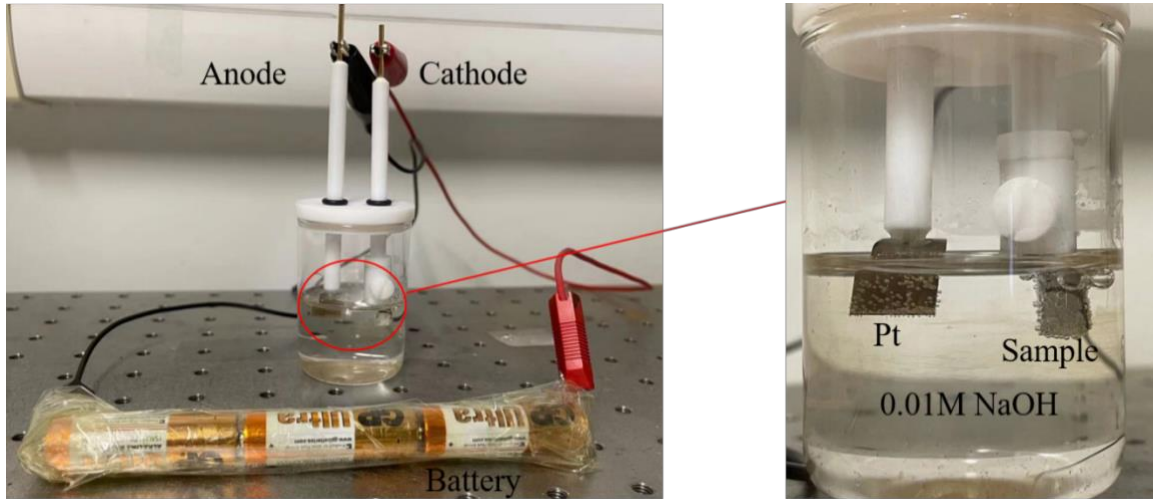
Figure 2.8 Experimental setup for hydrogen charging in 0.01M NaOH solution, where Pt as anode and the TiO$_2$ sample as cathode form an electric loop under 4.5 voltage.

The generation of hydrogen gas on the sample can be written as[54]

$$H_2O + e^- \Rightarrow OH^- + H_{charging}$$

$$H_{charging} + H_{charging} \Rightarrow H_2$$
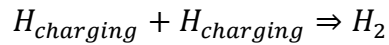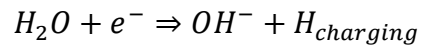
where $H_{charging}$ represents a hydrogen-charged atom. In previous research, it was demonstrated that hydrogen atoms diffused into the ceramics and caused reduction reactions [55]. During hydrolysis, hydrogen ions reduced Ti ions from Ti^{4+} to Ti^{3+}, accompanying a darkening in the appearance of TiO$_2$ crystal. A possible mechanism can be expressed as[56]

$$H_{charging} + Ti_{Ti} \Rightarrow H_i^{\cdot} + Ti_{Ti}'$$
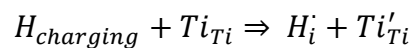
where $H_i^{\cdot}$ represents a hydrogen ion in the interstitial site. The electron in Ti_{Ti}' is a weakly

bonded electron acting as a charge carrier while an electric field is applied.

2.6 Electrodes

To observe the effect of light on the flexoelectricity, the conductive electrode coated on the

sample surface should be transparent. In my project, I selected semi-transparent gold

electrodes deposited by dc sputtering. The Au electrode was deposited by sputtering at base

vacuum condition of 1×10^{-3} Torr filled with Ar gas with a partial pressure of 5×10^{-3} Torr,

and the dc voltage of sputtering is 6.0 kV. The deposition time is controlled at 30 sec.

resulting in the semi-transparent Au film with a thickness estimated as 5-10 nm. The

absorbed light intensity of the crystal was measured by a photodetector. These experiments

were performed with the rest of the laboratory in dark.

We chose Au instead of ITO because the film formed by Au sputtering on the upper

and lower surfaces is more uniform and symmetrical than the film formed by sputter-

deposited ITO films. Coating of Au electrode avoids heating and annealing process used

for ITO electrode coating which is not suitable for samples such as hydrogen doped TiO_2

since hydrogen will escape from the sample.

Chapter III

Enhanced flexoelectricity in SrTiO$_3$ crystal

3.1 Introduction

The coupling between flexoelectricity and photovoltaics (PV), as one of the most promising phenomena from the application point of view, has triggered many investigations and discussions in the flexoelectric community. Yang *et al.* firstly raised the idea of the flexo-photovoltaic effect, where the strain gradient induced polarization in centrosymmetry materials could induce PV effect analogous to ferroelectric PV effect.[14] Later on, Shu *et al.* discovered that ultraviolet light (UV) can enhance the flexoelectricity by two orders of magnitude for hybrid perovskites, and they further proved that such photo-flexoelectricity can be a general property of semiconductors.[57] Recently, controllable photoconductance in a freestanding BiFeO$_3$ membrane was demonstrated by Guo *et al,*[58] extending the research of photoflexoelectric effect to thin films. Though more studies are showing the effective coupling between flexoelectric and photoelectric properties, there still lacks a clear physical picture describing the flexo-photovoltaic effect, where the interactions between photon, charge, and polarity make the mechanism more complicated.

Photo-enhanced flexoelectricity or flexoelectricity-enhanced photovoltaic effect, named photo-flexoelectric is an interesting topic and has application potential in photo-

electro-mechanical devices. However, this effect is far from being well understood. In this work, we demonstrate the photo-flexoelectric effect in perovskite structured STO single crystal and reveal the coupling mechanism between its photovoltaic and flexoelectric effect. Driven by the flexoelectric field, light-induced electrons can tunnel through the Schottky junction at the Au/STO interface, giving rise to enhanced flexoelectricity, i.e., photo-flexoelectric effect. Thermal annealing in vacuum induces oxygen vacancies in STO and results in stronger light absorption and enlarged photo-flexoelectric effect.

As the photoflexoelectric effect has been observed in STO,[61] this cubic structured perovskite could be a good platform to investigate the coupling between flexoelectricity and photovoltaics. We are also motivated by the fact that oxygen vacancy density in materials can influence their flexoelectric property; as reported, three orders of magnitude larger flexoelectric coefficient has been reported in reduced $BaTiO_3$ single crystal.[7] It is known that after high-temperature vacuum annealing, STO single crystal shows distinct electrical transport property change through the accumulation of oxygen vacancies.[59] Therefore, it is expected that stimulated by both light illumination and oxygen vacancies, a large flexoelectric response could be achieved in STO crystal.

3.2 Experimental details

Two-side polished STO single crystal plates with a thickness of 0.5 mm used in this work are from MTI Corporation, and the bare crystals were cut into a beam shape with a size of 5×10 mm^2. Semitransparent gold electrodes of ~5 nm thick were sputter deposited on the two surfaces of STO plates forming a capacitor structure (electrode/STO/electrode). To measure flexoelectricity, a piezoelectric actuator was used to deliver an oscillatory force to the free end of clamped cantilever-shaped crystals, and the alternating current induced by the oscillatory bending was measured with a lock-in amplifier connected to the electrodes with coaxial cables. Using standard elastic deformation equations, for a point-loaded single-clamped beam, the strain gradient was calculated from the deflection amplitude and the distance from the clamped side and actuator contact point, and the polarization was extracted from the amplitude of the oscillating current and the frequency of the actuator. The linear proportionality constant between polarization and strain gradient is the flexoelectric coefficient. To measure the photocurrent, the same setup was used, and the DC induced by UV light was measured with a KEITHLEY 2400 source meter.

The light absorption spectrum of the STO sample with Au electrodes at the two surfaces was measured to determine the optimal wavelength range. It shows that 365 nm wavelength UV light can be well absorbed by STO. This result also indicates that the light intensity at the top surface is a few times of magnitude stronger than the bottom surface. Therefore, the photocurrent generated from the top surface dominates the process.
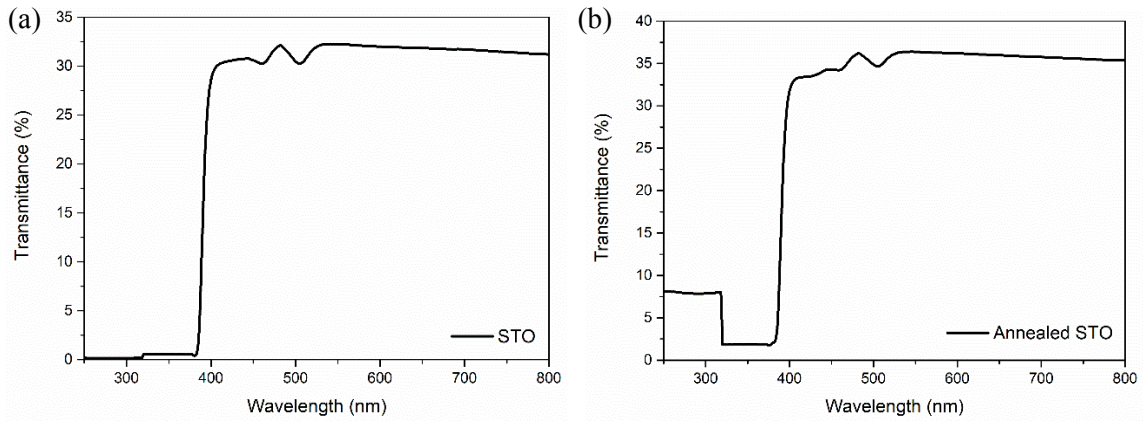
Figure 3.1 Optical transmission spectra of pristine (a) and annealed (b) STO crystal with

Au electrode at top and bottom surfaces.

3.3 Enhanced Flexoelectricity by Annealing

The u-bending and n-bending describe the bending geometry with the reference of the direction of light illumination, as illustrated in Fig. 3.2, wherein in both bending cases, light illuminates the top electrode. To introduce oxygen vacancies in STO, the bare crystals were thermally annealed in a 10^{-5} Pa vacuum at 700ºC for 2 hours. As shown in Fig. 3.2, a slightly darker appearance can be seen from the annealed sample. A UV laser with a 365 nm wavelength was used to induce the photoelectric effect, while the light intensity was calibrated with 3A-P-FS-12 (thermal power/energy laser measurement sensor) and StarLite P/N 7Z01565 (Low-Cost Portable Laser Power & Energy Meter).

The effective flexoelectric coefficient of (001) STO single crystal with semitransparent Au electrodes on both sides was measured in dark and under UV illumination. The polarization under different strain gradients is shown in Fig. 3.2, where the labeled flexoelectric coefficients are calculated from the slope of the fitting lines. As shown in Figs. 3.2 (a) and (b) which are for the n- and u-shape bending of the pristine STO crystal, respectively, the effective flexoelectric coefficient of the STO in dark is about 1 nC/m. Under a vertical illumination by UV light from the top surface, as shown by the red lines in Figs. 3.2(a) and 3.2(b), the flexoelectric coefficients increase by a few times.

We then measured the effective flexoelectric coefficients of the annealed STO (or called reduced STO since XPS result reveals reduction of Ti^{4+} to Ti^{3+} as shown in Fig. 3.3), and the results are shown in Figs. 3.2(c) and (d). It is interesting to see that, compared to the pristine sample, the flexoelectric coefficient of the reduced STO shows one order of

magnitude increment and a more significant enhancement under UV illumination. Integrating both effects from UV illumination and annealing, the flexoelectric coefficient of STO is greatly enhanced by more than two orders of magnitude, i.e. a strong photoflexoelectric effect which is independent of bending directions.
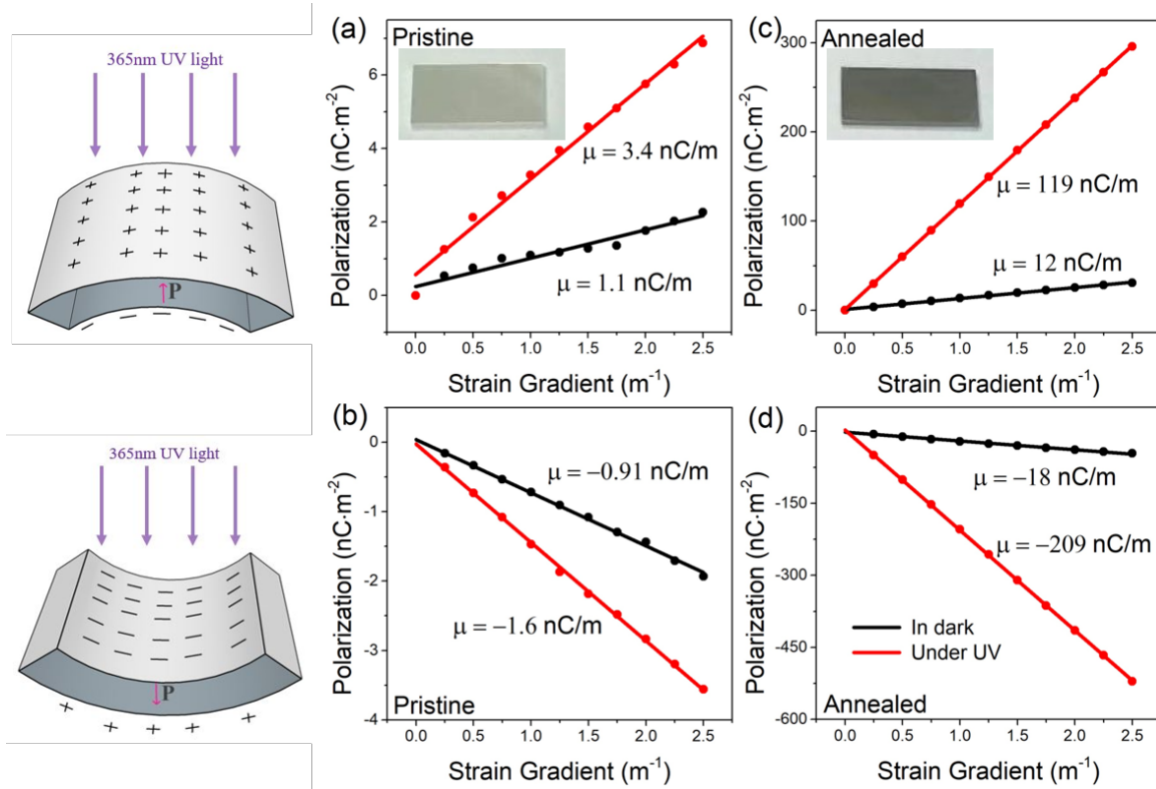
Figure 3.2 Enhanced effective flexoelectric effect under UV light incident from the top surface of sample: (a) pristine STO under n bending, inset: the photo of the as-received pristine STO crystal, (b) pristine under u bending, (c) annealed STO sample under n bending, inset: the photo of the annealed STO crystal, and (d) annealed STO sample under u bending.

To confirm the formation of oxygen vacancies in STO, we conducted XPS characterization to the annealed STO sample. The results in Fig. 3.3 show the degradation of Ti valence states from 4+ to 3+, which proves the formation of oxygen vacancies.
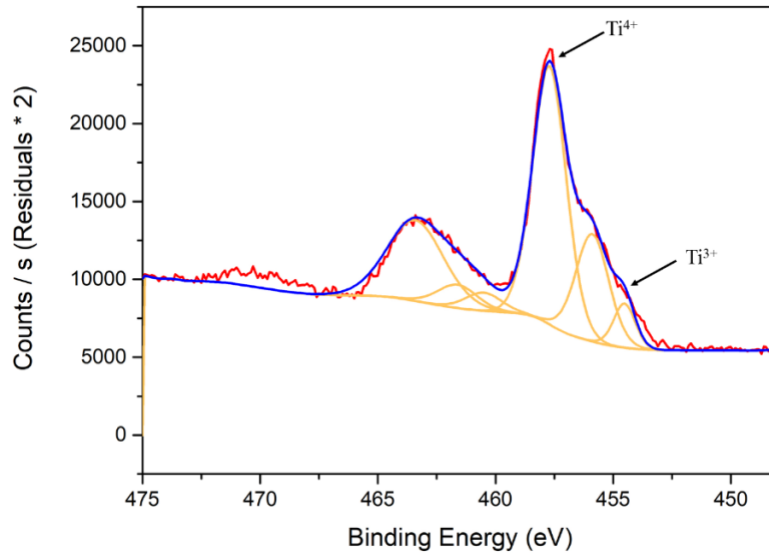
Figure 3.3 XPS spectrum of annealed STO at 700 ºC for 2hrs in vacuum showing the degradation of Ti valence states from 4+ to 3+.

3.4 Barrier layer model

According to the barrier layer model,[60] the photoflexoelectric enhancement could be attributed to the narrowing of the depletion width of the Schottky barrier at the Au/STO interface. In our experiment, both light illumination and induced oxygen vacancies can increase the charge carrier concentration in STO and further shrink the width of the depletion region. A quantitative dependence of the effective flexoelectric coefficient of semiconducting materials is given by [57]

$$\mu_{\text{eff}} \equiv \sqrt{\frac{n\varepsilon_0\varepsilon_r}{2\phi_0}}\,\varphi\,\frac{t}{2} \tag{3.1}$$

where n is the free carrier concentration, ε_r the relative dielectric constant, ϕ_0 the Schottky barrier height, φ the surface deformation potential, and t the sample thickness. If we assume the change of the free charge carrier concentration dominates the change of μ_{eff} in our experiment, the flexoelectric enhancement for the reduced STO in dark corresponds to two orders of magnitude increase of the free carrier concentration. As shown in Fig. 3.2, a much larger increment of μ_{eff} was observed on the annealed STO sample. This can be attributed to the presence of charged oxygen vacancies in the STO crystal, where the defect levels lower the Fermi level of STO and decrease the Schottky barrier at the interface and then result in a much higher μ_{eff} in Eq. 3.1.

We have conducted Hall measurement on the STO samples, but both pristine and 700°C vacua (2x10^{-5} Pa) annealed samples show too high resistance for carrier concentration measurement. Alternatively, we measured the sheet carrier concentration of

550°C annealed STO sample with AlN capping layer which is $1.2 \times 10^{15}/cm^2$ at room temperature. This carrier concentration is generally within the range of the carrier concentration of the reduced STO substrate in a two-dimensional electron gas-like system.[61] It has been reported that 1200°C vacuum annealing results in an average electron carrier concentration of $5 \times 10^{15}/cm^3$, and it has also been demonstrated that when exposed to UV light, the electron carrier concentration in the annealed sample increases by two orders of magnitude. [62] Therefore, the increased electron carrier concentration in the annealed sample and its further boosting by UV light should be responsible for the increased flexoelectricity.

Based on the Hall measurement, the annealed STO shows an n-type characteristic, and it exhibits a room temperature sheet carrier concentration of $1.22 \times 10^{15}/cm^2$, with electron mobility of $0.758\ cm^2/Vs$. The resistance of the pristine sample is too high to allow any carrier density measurement by the Hall method. The significantly increased carrier density for the annealed sample should be responsible for increased flexoelectricity. Figure 3.4 shows our measurement results (carrier density and mobility) at different temperatures.
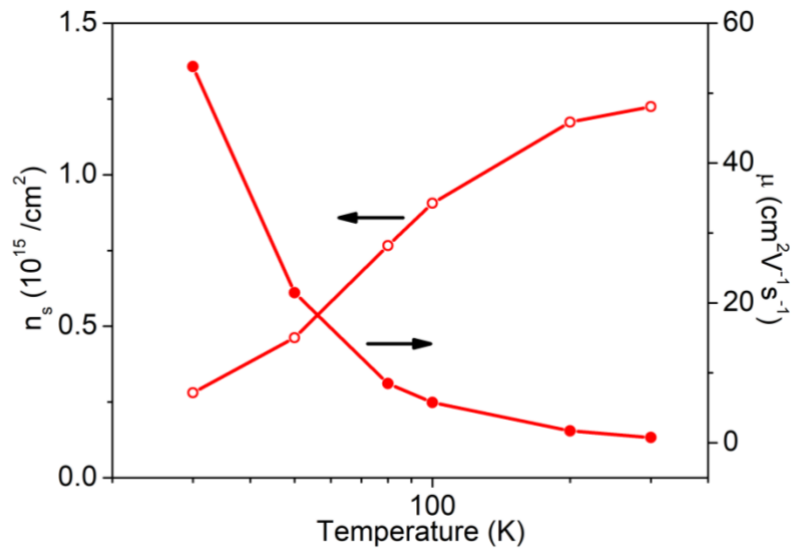
Figure 3.4 Sheet carrier density and mobility at different temperatures for the annealed STO sample.

3.5 Photo-flexoelectric effect

To understand the giant photo-flexoelectric increment more comprehensively in STO, we studied the dependence of flexoelectric current on light intensity. As shown in Fig.3.5, for both the pristine and annealed STO samples, the flexoelectric current increases gradually with the increase of the UV light intensity. The increase of flexoelectric current in correlation with UV intensity increase suggests that the extra flexoelectric signal comes from the photo-excited carriers in the STO crystal. Furthermore, the nonlinear response of flexoelectric current fits well with the theory of photoresponse which gives a power law:

$$I = \alpha L^\beta \tag{3.2}$$

where α is a constant, L the light intensity, and β empirical power value is related to the photosensitivity of the sample and indicates the efficiency of generating charge carries by light. [63,64] From the fitting curve shown in Fig. 3.5, the β value is about 0.24-0.25 (Figs. 3.5 (a) and (b)) for the pristine sample and 0.30-0.35 (Figs. 3.5 (c) and (d)) for the annealed sample. The higher empirical power value of the annealed sample suggests that it has a more sensitive photo-responsivity than the pristine sample. Referring to Eq. 3.1, where the flexoelectricity is proportional to $n^{1/2}$ of the charge carrier density if, with β=0.25 and 0.35, the photogenerated charge carrier densities should have a relationship with incident light intensity as $n\sim L^{0.5}$ and $L^{0.7}$, respectively, for the pristine and annealed samples. We note that such a nonlinear light-intensity dependent property, i.e., the non-unity exponent, has also been observed in many nanostructure-based photodetectors, such as ZrS_2 nanoribbons,[65] CdTe nanoribbons,[66] CuO nanowires,[67] In_3S_3 nanowires,[68]etc., which is a

result of the complex processes of electron-hole generation, trapping, and recombination in the semiconductor.[69, 70]
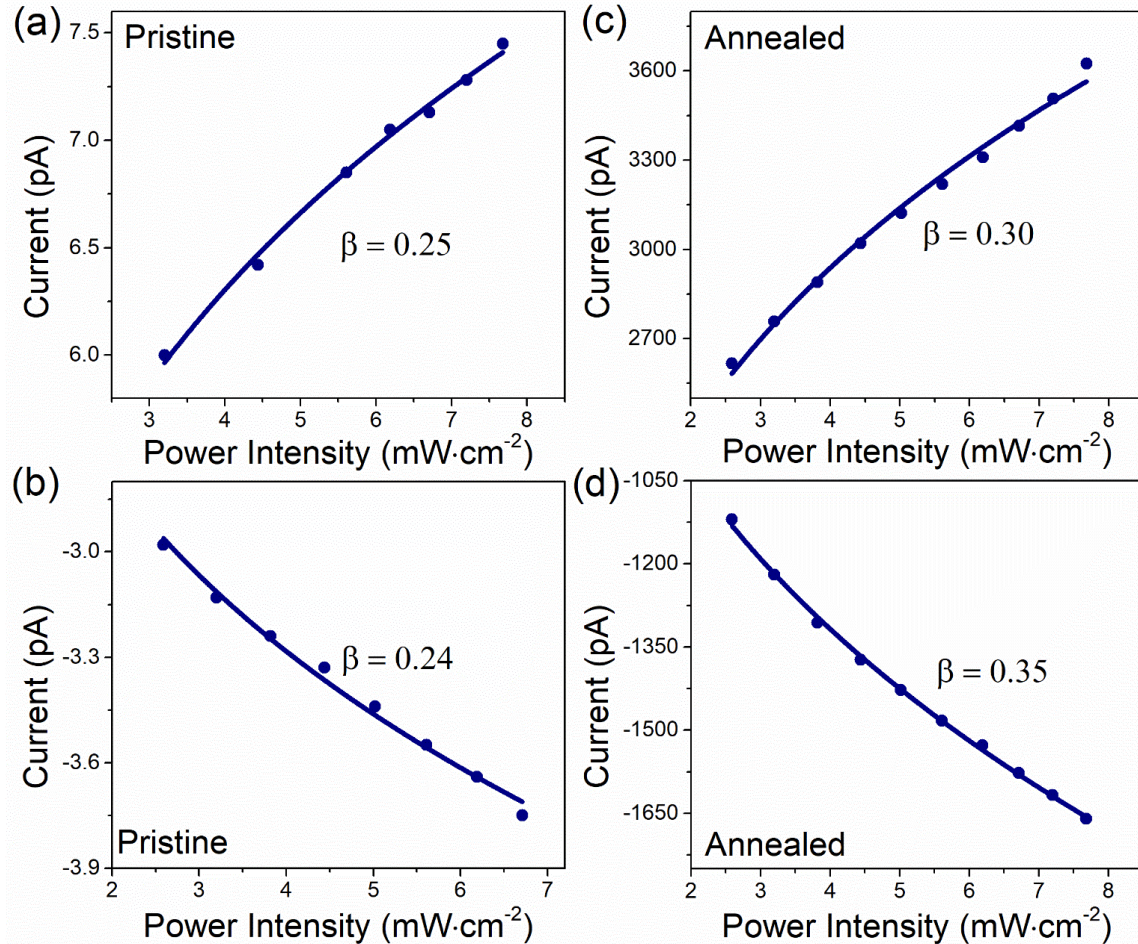
Figure 3.5 Light-intensity dependence of flexoelectric current under a constant strain and increased UV light incident from top of the sample surface: (a) pristine STO under n bending, (b) pristine under u bending, (c) annealed STO sample under n bending, (d) annealed STO sample under u bending. The fitting curves are with the power law.

For the same bending model, strain gradient dependence of flexoelectric currents under a constant light intensity and increased strain gradient is shown in Fig. 3.6. This

experiment illustrates that similar β power values are tested for different strain gradients, which means that power value might be the property for dielectrics.
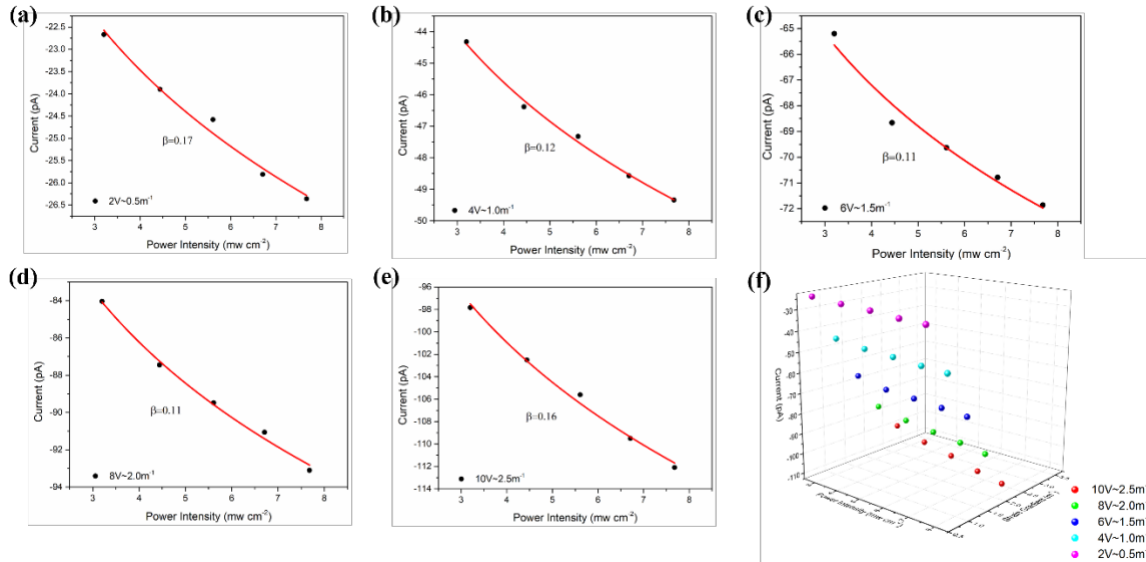
Figure 3.6 Strain gradient dependence of flexoelectric current under a constant light intensity and increased strain gradient. The notation 2,4,6,8,10V represents the amplitude of driving voltage of the vibrator which corresponds to strains of 0.5, 1.0, 1.5, 2.0, and 2.5 /m, respectively.

3.6 Photocurrent

To further demonstrate the generation of charge carriers in STO, we measured the photocurrent at the Au/STO interface, and the results are shown in Fig.3.7. The generation of photocurrent when UV light incidents to the top surface area are due to the Schottky junction formation at the interface of Au/STO; while the absorption of light (see Fig. 3.1) by the crystal makes the bottom surface of the crystal illuminated with much weaker light, therefore the junction at top surface dominates the photocurrent (otherwise the symmetric electrodes on top and bottom will result in zero photocurrents).
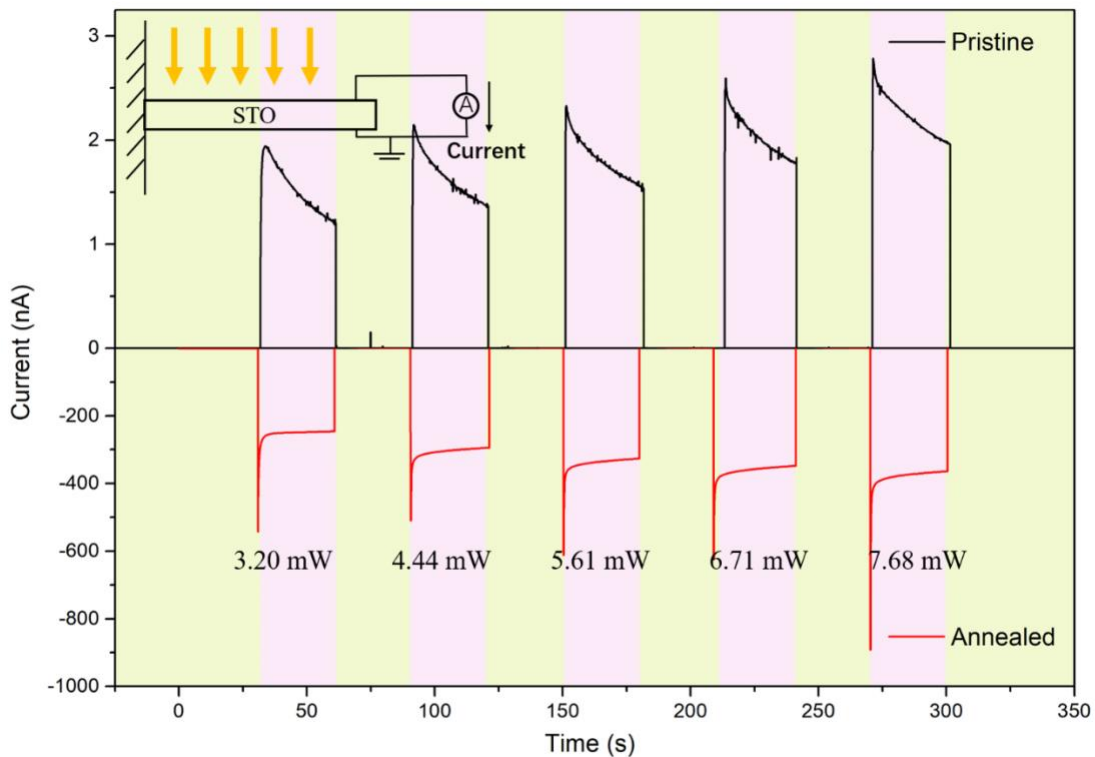
Figure 3.7 Photocurrent of pristine and annealed STO samples. The annealed sample shows an enhanced and reversed photovoltaic effect.

It is well-known that STO is a good insulator, but the positive photocurrent for the pristine STO suggests its weak p-type semiconducting nature due to the possible existence of Sr or Ti vacancies from non-perfect chemical stoichiometry during crystal growth at very high temperatures. It has been reported that 1000 °C annealing can induce Sr vacancies leading to p-type semiconducting of STO,[71,72,73] and the corresponding energy band diagram between Au and p-type STO is shown in Fig. 3.8 (a).

It is interesting to see from Fig. 3.7 that the photocurrent of the reduced STO is two orders of magnitude larger than the pristine sample and the photocurrent is negative in contrast to the positive photocurrent for the pristine sample. The significant increase of photocurrent for the annealed sample is due to the oxygen vacancy-induced defect levels as light absorption centers which convert photon energy to electron-hole pairs. The change of sign of the photocurrent can be understood by the fact that the annealed STO is an n-type semiconductor, which is well-known, resulting in Schottky junction as shown in Fig. 3.8(b). In our experiment, the 700 ºC annealing in a vacuum is a condition to reduce the STO crystal by introducing many oxygen vacancies. Oxygen vacancy induces the extra level 0.2 eV below the conduction-band maximum (CBM) in the bandgap,[27] thus the STO crystal changes from p-type to n-type conducting.

It should be noticed that the photocurrent is a persistently decayed current under constant light and will not contribute to the alternative flexoelectric current measured by lock-in. However, as illustrated in Figs. 3.8 (c) and (d), driven by the alternative flexoelectric field, light-induced electrons can tunnel through the Schottky junction at the Au/STO interface, giving rise to enhanced flexoelectricity, i.e., photo-flexoelectric effect.

Flexoelectric polarization attracts photo-induced carriers and bending-induced electrons near the interface, resulting in a reduced interfacial energy barrier. This photo-enhanced flexoelectricity is independent of bending directions (n and u-shape bending) which can be seen in Figs. 3.2 and 3.5. On the other hand, we did not see a clear enhancement of the photovoltaic effect when we bent the sample; this is because the contribution of the flexoelectric field to the charge transfer across the Schottky junction is much smaller compared to the photocurrent which is two orders of magnitude larger than flexoelectricity induced current.
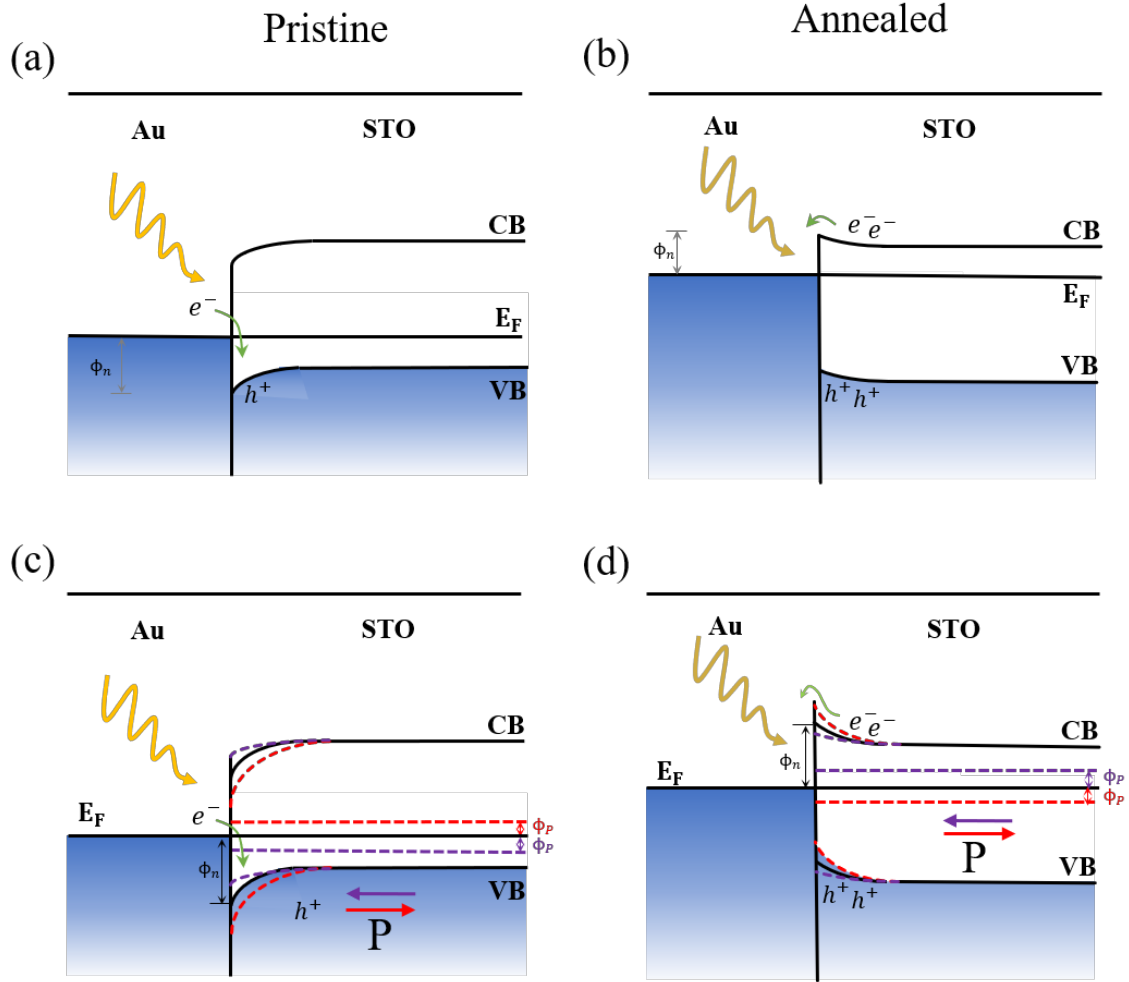
Figure 3.8 *Energy band diagrams and electron tunneling at the Au/SrTiO₃ interface for pristine (a) and annealed (b) STO samples. (c) and (d) are the corresponding energy band diagrams and electron tunneling with the presence of flexoelectric polarization indicated by arrows. CB, energy pf conduction band minimum; VB, energy pf valence band maximum; E_ϕ, vacuum energy. P represents the flexoelectric field.*

3.7 Switchable diode effect in oxygen vacancy modulated SrTiO₃ single crystal

In non-ferroelectric STO, the switchable diode effect has been studied, showing that the switching of diode could be explained by a new mechanism related to the migration of oxygen vacancies after a sweeping voltage. Additionally, a self-compliance property of resistive switchable diode effect has been observed.

To further understand the oxygen vacancy behavior, the vacuum annealed STO was tested with I-V curve measurement by applying sweeping voltages from -10 V to 10 V. As shown in Fig 3.9, the sequence of the voltage sweeping is from 0 V to a maximum of positive voltage 10 V and then to a maximum of negative voltage -10V, and finally back to 0 V. One can see that a diode behavior for annealed STO is presented.
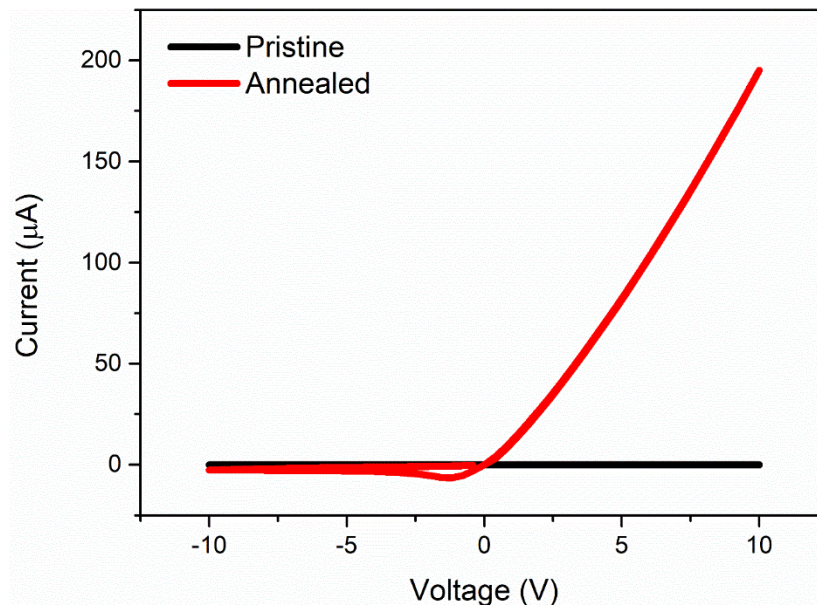
Figure 3.9 The I-V curves of the annealed and pristine STO within the range from -10 to 10 V.

Based on the appearance of switchable diode behavior, Pan[74] has proposed a mechanism that the generation of oxygen vacancies in samples converts STO insulators to n-type semiconductors. The results of XPS measurements (Fig. 3.3) and hall measurements (Fig. 3.4) show that oxygen vacancies generated during annealing are distributed near the surface of the STO single crystal. The generation of the oxygen vacancies accompanied by electrons is donated into the conduction band, resulting in the oxygen vacancies being regarded as donors.[75]

After switching the anode and cathode, Fig. 3.10 shows the negative diode-like curve ranging from -10V to 0V, opposing the baseline. This phenomenon shows that the oxygen vacancies are not uniformly distributed in the sample but have a certain directionality.
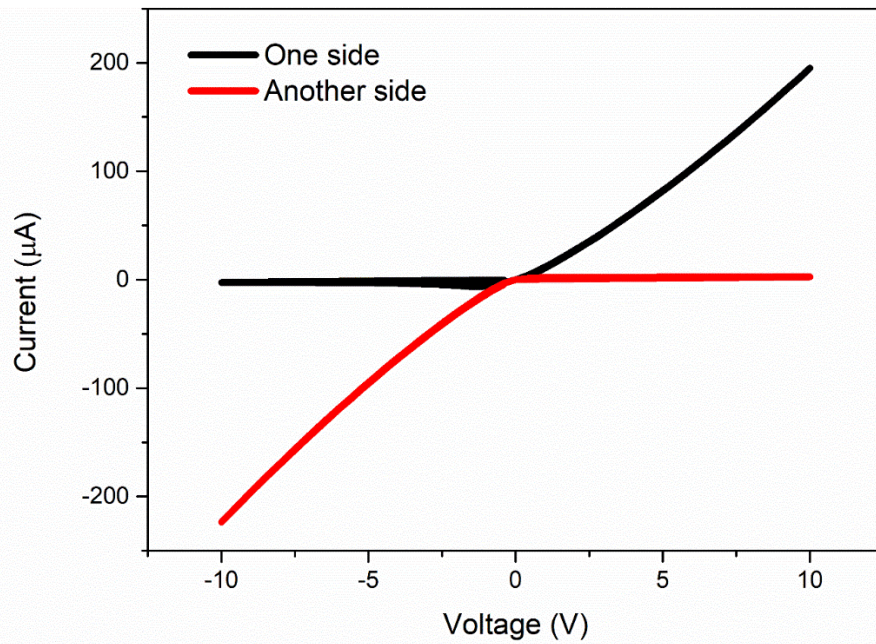
Figure 3.10 The I-V curves of the one side and another side STO within the range from -10 to 10V.

Pan *et al* proposed that if the voltage in the opposite direction is applied, the concentration of oxygen vacancies in different positions can be changed. Therefore, after a +20 and -20 DC voltage is applied, Fig. 3.11 shows that the I-V characteristic in (a) is opposite to that in (b). To explain the resistive switching behavior, a model of the n-n$^+$ junction and n$^+$-n junction correspond to the distribution of the oxygen vacancies after 20 and -20 DC voltage sweeping, respectively, were proposed.
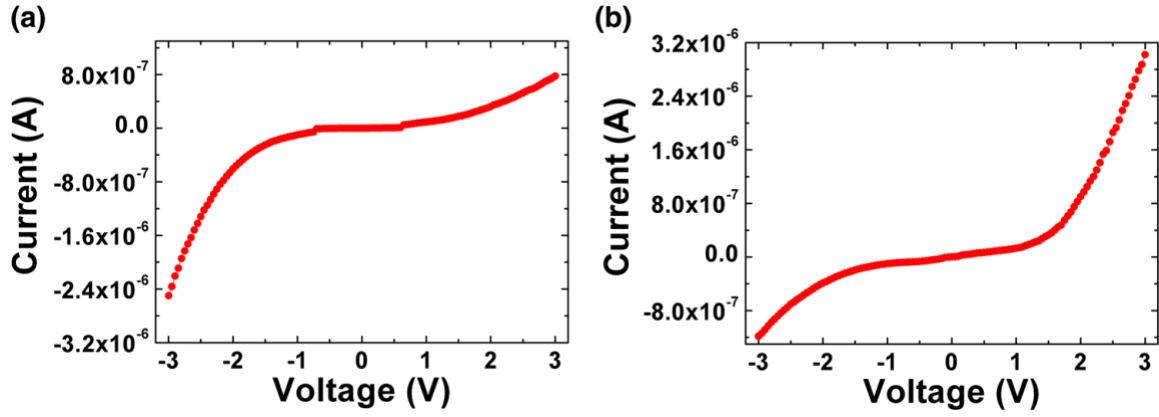
Figure 3.11 The I-V curves of the annealed STO capacitors within the range from -3 to 3V after 20 (a) and -20V (b) sweeping, respectively.[80]

3.8 Doping enhanced flexoelectricity

Nb-doped SrTiO$_3$ single crystal has attracted more attention since it is a good semiconductor. A study of its flexoelectricity can provide more information to understand the doping effect to the enhancement of the flexoelectric effect. Figure 3.12 shows the flexoelectric measurement of polarization under different strain gradients of Nb: STO with u-bending and n-bending (description of the bending geometry). The labeled flexoelectric coefficients are calculated from the slope of the fitting lines, where for the n- and u-shaped bending of the Nb: SrTiO$_3$ crystal, they are 756 nC/m and -496 nC/m, respectively. While as a reference, the effective flexoelectric coefficient of the STO is about 1 nC/m.

Our results show that, due to the doping effect, the flexoelectric coefficient of Nb: SrTiO$_3$ is greatly enhanced by more than two orders of magnitude compared to pristine STO, i.e. a strong doping-flexoelectric effect which is independent of bending directions. Doping increases the concentration of charge carriers in crystals, and if we assume the change of the free charge carrier concentration dominates the change of μ_{eff} in our experiment, the flexoelectric enhancement for the doping STO in dark corresponds to two orders of magnitude increase of the free carrier concentration. However, it should be pointed out that there is no correlation between light (including UV light) and the flexoelectricity of Nb: SrTiO$_3$. This could be due to the fact, that the Nb doing enhanced the flexoelectric effect much larger than the light effect (5-7 times larger).
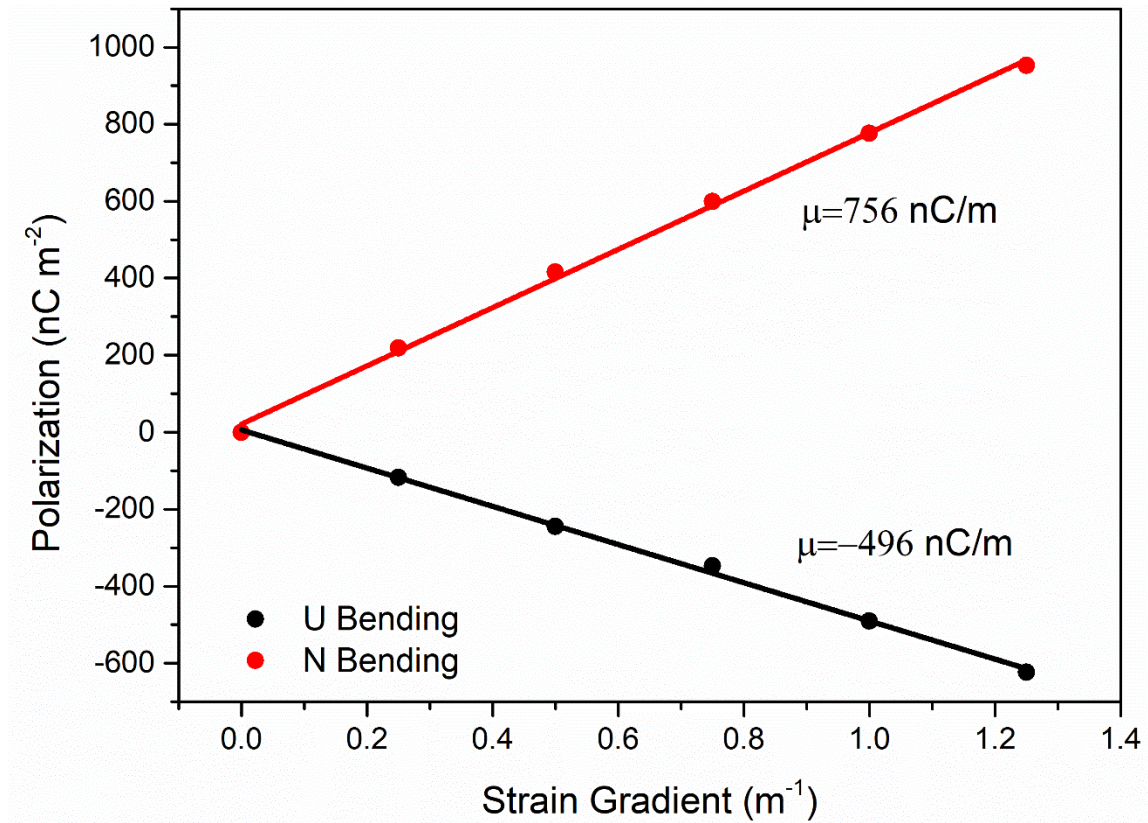
Figure 3.12 Enhanced flexoelectric coefficient due to Nb doping when Nb: SrTiO₃ single crystal is bending under U bending (red line) and N bending (black line).

3.9 Hydrogen-doping enhanced flexoelectricity

Two-side polished STO single crystals used in this work are from Hefei Crystal Technical Material Corporation, Limited, and the bare crystals were cut into a beam shape with a size of 10x3x0.26 mm^3. Polished single crystals were immersed in a 0.01M NaOH solution and 4.5V voltages were applied without any metal electrode as cathode and a Pt electrode as anode for 48 hours. Semitransparent gold electrodes of 5 nm thick were sputter deposited on the two surfaces of STO plates forming a capacitor structure (electrode /STO/electrode).

The effective flexoelectric coefficient of hydrogen-charged STO single crystal with semitransparent Au electrodes on both sides was measured. The polarization under different strain gradients is shown in Fig. 3.13, where the labeled flexoelectric coefficients are calculated from the slope of the fitting lines. As shown in Fig. 3.13 which are for the u-shape bending of the pristine and hydrogen-charged STO crystal, the effective flexoelectric coefficient of the 10x3x0.26 mm^3 pristine STO in dark is about 3.7 nC/m. The enhancement of flexoelectric coefficient for the hydrogen-charged STO (two times larger) is not as large as Nb doping or oxygen vacancy doping which show at least two orders of magnitude enhancement. This could be due to the difficulty of inducing a high concentration of hydrogen ions into the STO crystal.
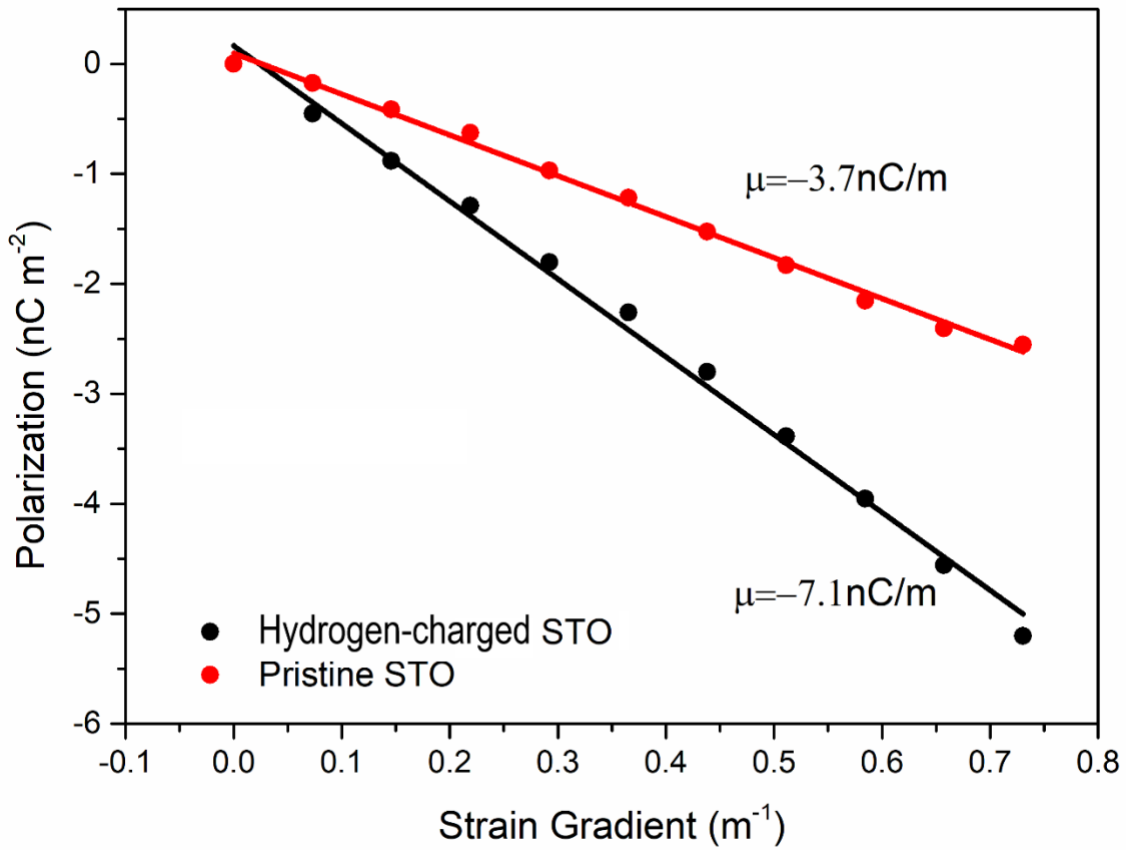
Figure 3.13 Enhanced flexoelectric coefficient due to hydrogen charging when SrTiO₃ single crystal is bending under U bending.

3.10 Summary

In summary, the photoflexoelectric effect has been studied in STO crystals. In this work, we compared the pristine, doped, and high-temperature annealed STO single crystals' flexoelectricity and their response to incident UV light, and we revealed coupling between the flexoelectric field, photo-induced current, and oxygen vacancy induced defects. It is found that by introducing UV light stimulations and oxygen vacancies and hydrogen and Nb in STO, the effective flexoelectric coefficient can be enhanced by more than double to two orders of magnitude, compared with the stoichiometry ones. These results help us to understand the mechanism of flexoelectricity and the photoflexoelectric effect and may provide hints of more correlation effects between flexoelectricity and photon-charge interaction. The increased flexoelectric coefficient may also have application prospects like energy harvesters, light sensors, and accelerometers. The increased flexoelectric coefficient may also have application prospects like energy harvesters,[76] light sensors,[77] and accelerometers.[78,79]

Chapter IV

Enhanced flexoelectricity in Hydrogen-charged TiO$_2$ single crystal

4.1 Introduction

Recently, the reactions between hydrogen and metal oxide materials have drawn much attention.[80,81,82] Hydrogen incorporation is a common technique to increase charge concentration in oxide materials, resulting in decreased resistance but also with increased dielectric loss[83]. In instance, hydrogen-charged anatase TiO$_2$ crystals in nanoscale have significantly enhanced photocatalytic performances, as reported by Chen *et al.*[84] Furthermore, hydrogen-charged TiO$_2$ nanocrystal arrays exhibited excellent photoelectrochemical performance through water electrolysis.[85] However, the proposed mechanisms for the above behaviors diverge in different research. For the reduction of bandgap of TiO$_2$, the interstitial hydrogen[86][87] regarded as the main reason rather than surface disorders[88][89] to improve its absorption ratio in visible light range. This hydrogen-induced degradation in oxide-based materials and devices is usually permanent and stable at room temperature. However, compared to vacuum annealing degradation, which is a recovery process,[90,91] hydrogen-induced defects are only metastable in TiO$_2$-based ceramic

capacitors at room temperature. Defects induced by hydrogen incorporation in many other oxides are gradually recovered during an aging process without any thermal treatment.[92]

The coupling between flexoelectricity and doping, as one of the most promising phenomena from the application point of view, has triggered many investigations and discussions in the community of flexoelectricity-related research. The doping of oxygen vacancies induced by high-temperature annealing can enhance the flexoelectricity of $SrTiO_3$,[93] and we expect hydrogen ions are analogous to oxygen vacancies and can also increase the flexoelectricity of metal oxides. Beyond, the hydrogen ions movement driven by flexoelectric field may also enhance the effective flexoelectricity.

As the resistive switching diode effect has been observed in high-temperature annealed TiO_2[94] , the hydrogen-charged TiO_2 could also be a good platform to investigate the coupling between flexoelectric and diode effects. We are also motivated by the fact oxygen vacancy density in materials can influence the electroforming behavior of metal oxide such as TiO_2.[76] Therefore, it is expected that stimulated by hydrogen ions, a large flexoelectric response could be achieved in TiO_2 crystal, and hydrogen ion density in the crystal should influence their flexoelectric property.

In this work, the flexoelectricity of pristine and hydrogen-charged TiO_2 single crystals and their response to a bias voltage are compared, and coupling between the flexoelectric filed and photocurrent as well as hydrogen ions induced defects are revealed. These findings can help us to understand the flexoelectricity and resistive switching diode effect and may extend present memory technologies.

4.2 Flexoelectricities of hydrogen-charged TiO$_2$ crystals

Two-side polished TiO$_2$ single crystals plat with a thickness of 0.5 mm used in this work are from MTI Corporation, and the bare crystals were cut into beam shape with a size of 7x10 mm^2. Polished rutile (001) single crystals were coated with a fired silver electrode at a corner of the sample as cathode, and then immersed in a 0.01M NaOH water solution for 168 hours with 4.5V voltage applied between the sample cathode and Pt anode electrode. Semi-transparent gold electrodes of 5 nm thick were sputter deposited on the two surfaces of the TiO$_2$ plates forming a capacitor structure (electrode/TiO$_2$/electrode). To measure the sample's flexoelectricity, a piezoelectric actuator was used to deliver an oscillatory bending force to the free end of a clamped cantilever-shaped crystal, and the alternating current induced by the oscillatory bending was measured with a lock-in amplifier connected to the electrodes with coaxial cables. Using standard elastic deformation equations, for a point-loaded single-clamped beam, the strain gradient was calculated from the deflection amplitude and the distance from the clamped side and actuator contact point, and the polarization was extracted from the amplitude of the oscillating current and the frequency of the actuator. The linear proportionality constant between polarization and strain gradient is the flexoelectric coefficient.

A PERKIN ELMER_UV-vis-NIR spectrometer was used to characterize the absorption spectra of the pristine and hydrogen-charged TiO$_2$ crystal samples. As shown in Fig. 4.1, the light absorption spectra of the pristine and hydrogen-charged TiO$_2$ samples with Au electrodes at the two surfaces were measured to determine the optimal wavelength range for photo-enhanced flexoelectricity. It is apparent that the hydrogen-charged TiO$_2$

crystal absorbs more light in all wavelengths than the pristine TiO_2, and both samples show strong absorption to UV light below 365 nm wavelength. This result also indicates that the light intensity at the top surface is a few times of magnitude stronger than the bottom surface. Therefore, the photocurrent generated from the top surface dominates the process. A UV laser with a 365 nm wavelength was suitable to induce the photovoltaic effect.
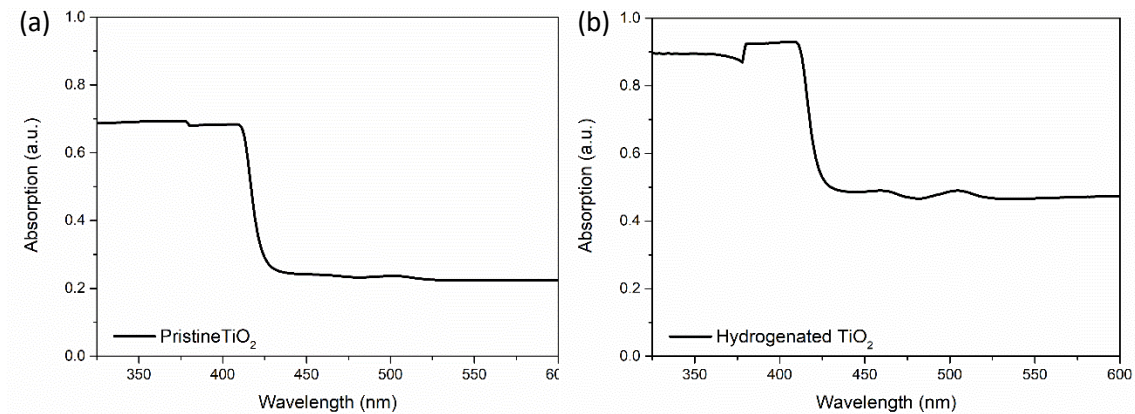
Figure 4.1 Optical transmission spectra of pristine (a) and hydrogen-charged (b) TiO_2 crystal.

To confirm the existence of hydrogen ions in TiO_2, we conducted Fourier Transform Infrared (FTIR) characterization of the hydrogen-charged TiO_2 sample. As shown in Figure 4.2, the absorption peak located at around 3280 cm^{-1} wavenumbers indicates the formation of O-H bonding, which proves the hydrogen identification[95]. The hydrogen-charged TiO_2 crystal becomes blue color but still transparent, also indicating the successful formation of O-H bonding in the TiO_2 crystal.
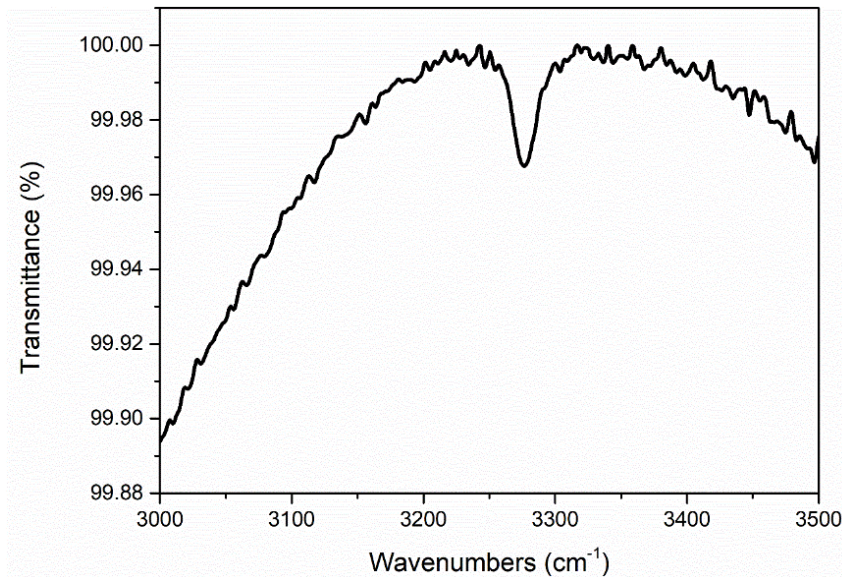
Figure 4.2 FTIR spectrum of hydrogen-charged TiO₂ showing the absorption by oxygen-hydrogen bonding.

The effective flexoelectric coefficients of (001) TiO_2 single crystals with semi-transparent Au electrodes on both sides were measured. The polarization under different strain gradients is shown in Fig. 4.3, where the labeled flexoelectric coefficients are calculated from the slope of the fitting lines. As shown in Fig. 4.3 (a) which is for the u-shape bending of the pristine TiO_2 crystal, the effective flexoelectric coefficient of the pristine TiO_2 in dark is about 1 nC/m; while for the hydrogen-charged TiO_2 sample, the flexoelectric coefficient is enhanced by more than two orders of magnitude.

The effective flexoelectric coefficients of the hydrogen-charged TiO_2 (or called hydrogen-doped TiO_2) crystal corresponding to the n- and u-shaped bending were also measured, and results are illustrated in Fig. 4.3 (b). It is apparent that the sample is macroscopically symmetric for the top and bottom surfaces, and there is no obvious

difference between the two bending modes in terms of the flexoelectric effect. To further demonstrate the generation of charge carriers in the hydrogen-charged TiO_2 crystal, the photocurrent at the Au/ TiO_2 interface was measured, and the results are shown in Figs. 4.3 (c) and (d). When UV light incidents to the top surface, the generation of photocurrent is due to the photovoltaic effect; while the absorption of light (see Fig. 4.1) by the crystal makes the bottom surface of the crystal illuminated with much weaker light, therefore the junction at the top surface dominates the photocurrent (otherwise the symmetric electrodes on top and bottom will result in zero photocurrents).

It is interesting to see from Fig. 4.3 that the photocurrent of the hydrogen-charged TiO_2 crystal is three orders of magnitude larger than that of the pristine crystal sample and the photocurrent is negative in contrast to the positive photocurrent for the pristine sample. The significant increase of photocurrent for the hydrogen-charged sample is due to the hydrogen ions induced defect levels within the bandgap as light absorption centers which convert photon energy to electron-hole pairs. The change of sign of the photocurrent can be understood by the fact that the hydrogen-charged TiO_2 is an n-type semiconductor.
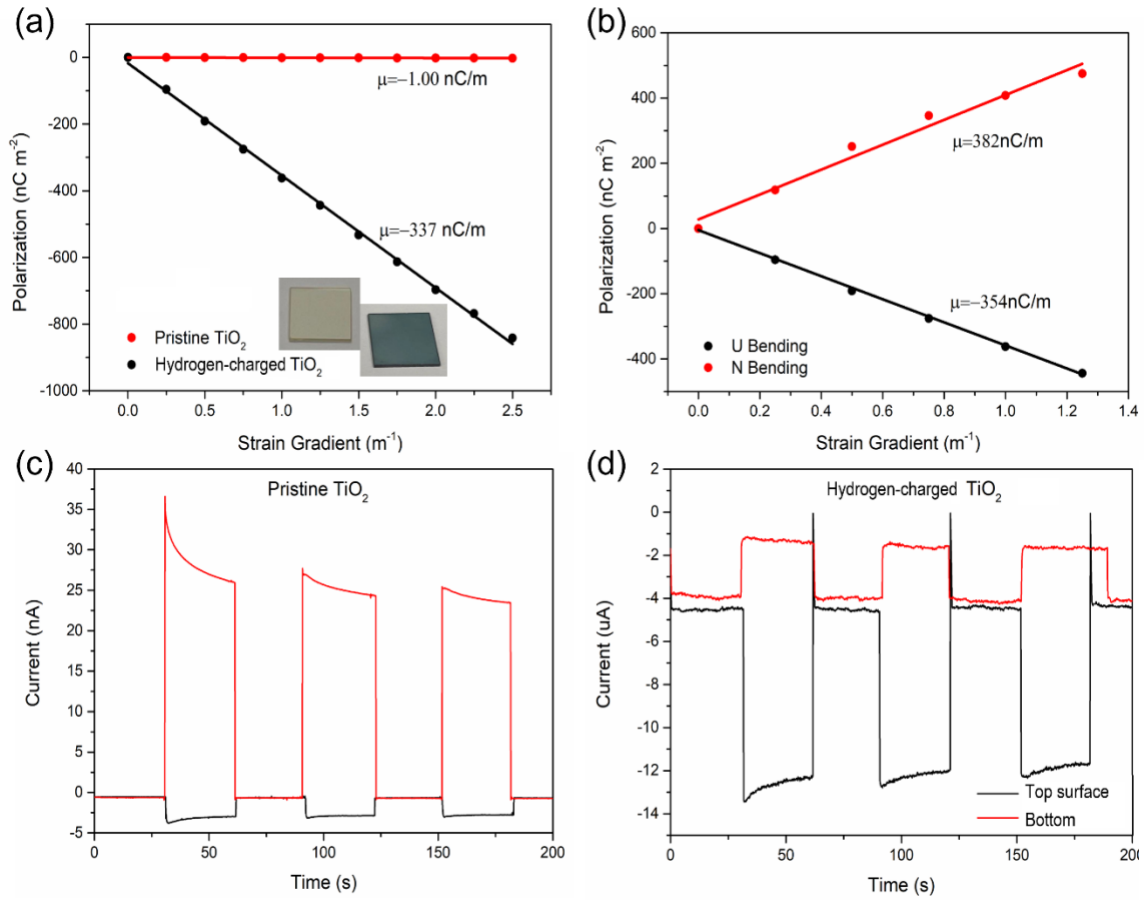
Figure 4.3 (a) Effective flexoelectric effect of pristine and hydrogen-charged TiO₂ crystals. (b) Comparison of the flexoelectric coefficients corresponding to n- and u-shaped bending for the hydrogen-charged TiO₂ crystal. (c) Photocurrent at the Au/TiO₂ interface for pristine and (d) hydrogen-charged TiO₂ crystals.

It should be noticed that the photocurrent is a persistently decayed current under constant light and will not contribute to the alternative flexoelectric current measured by the lock-in amplifier. However, as illustrated in Figs. 4.4 (a) and (b), light-induced electrons and holes can migrate to electrodes, giving rise to enhanced photocurrent, i.e.,

photovoltaic effect. Thus, the photocurrent of hydrogen-charged TiO_2 crystal is three orders of magnitude larger than that of the pristine sample. On the other hand, we did not see a clear enhancement of the photovoltaic effect when we bent the sample; this is because the contribution of the flexoelectric field to the charge transfer across the Schottky junction at the surface is much smaller compared to the photocurrent which is two orders of magnitude larger than flexoelectricity induced current.
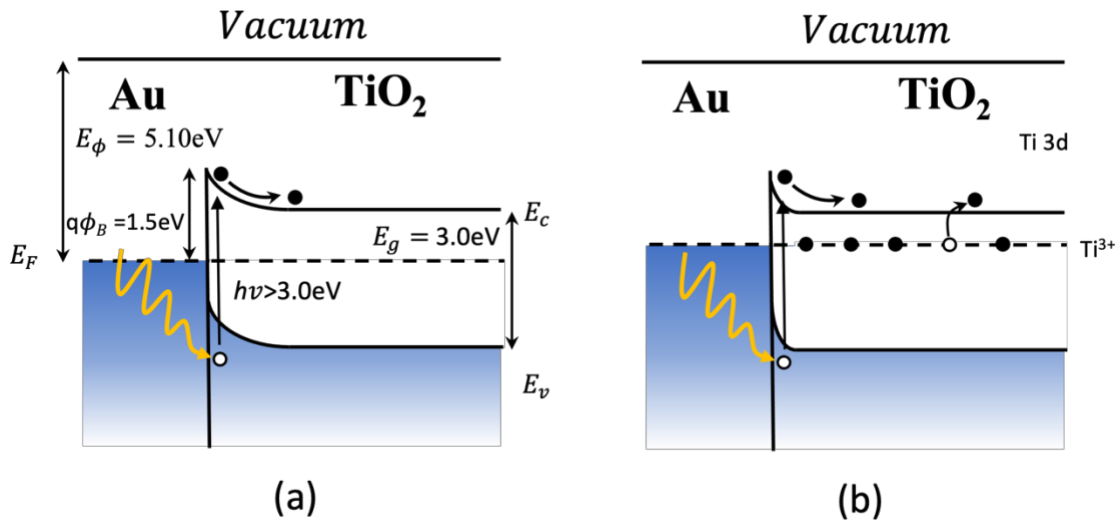
Figure 4.4 Energy band diagrams and electron tunneling at the Au/TiO₂ interface for pristine (a), and hydrogen-charged (b) TiO₂ crystals under UV light illumination. Ec, energy conduction band minimum, Ev, energy valence band maximum, and E_ϕ , work function.

To further understand the oxygen vacancy behavior, the hydrogen-charged TiO_2 crystal was tested with I-V curve measurement by applying sweeping voltages from -10 V to 10 V. As shown in Fig. 4.5(a), the sequence of the voltage sweeping is from 0 V to a

maximum of positive voltage 10 V and then to a maximum of negative voltage -10V, and finally back to 0 V. One can see that a loop behavior for hydrogen-charged TiO_2 is presented compared to the pristine TiO_2 crystal, indicating that the hydrogen ions can migrate driven by the external electric field and result in resistance change like a memory.

To prove the n-type conduction nature of the hydrogen-charged TiO_2 crystal, we also conducted the Seebeck coefficient measurement, and the results are shown in Fig.4.5b. One can see that the hydrogen-charged TiO_2 crystal is an n-type semiconductor. The increase of the Seebeck coefficient in the 2nd cycle of measurement is believed to be due to the out-diffusion of hydrogen ions from the crystal resulting in a decreased charge carrier. Usually, the Seebeck coefficient is reversely proportional to charge carrier density. A more detailed study is needed to understand its thermoelectric properties.
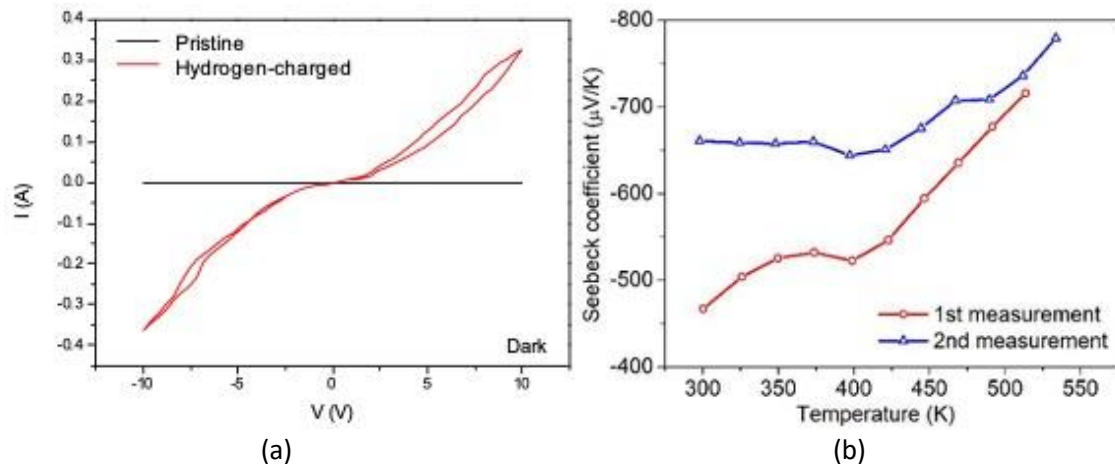

(a)   (b)

Figure 4.5 (a) The I-V curves of pristine (black line) and hydrogen-charged (red line) TiO₂ crystals. (b) The temperature-dependent Seebeck coefficient within the temperature range from 300 K to 550 K.

According to the barrier layer model,[96] the photo-flexoelectric enhancement could be attributed to the narrowing of the depletion layer of the Schottky barrier at the Au/TiO$_2$ interface. In our experiment, induced hydrogen ions can increase the charge carrier concentration in TiO$_2$ and further shrink the width of the depletion region. A quantitative dependence of the effective flexoelectric coefficient μ_{eff} of semiconducting materials is given by:[57]

$$\mu_{\text{eff}} \equiv \sqrt{\frac{n\varepsilon_0\varepsilon_r}{2\phi_0}}\,\varphi\,\frac{t}{2} \tag{4.1}$$

where n is the free carrier concentration, ε_0 the vacuum dielectric permittivity, ε_r the relative dielectric constant, ϕ_0 the Schottky barrier height, φ the surface deformation potential, and t the sample thickness. If we assume the change of the free charge carrier concentration dominates the change of μ_{eff} in our experiment, the flexoelectric enhancement for the reduced TiO$_2$ in dark corresponds to two orders of magnitude increase of the free carrier concentration. As shown in Fig. 4.3(a), a much larger increment of μ_{eff} was observed on the hydrogen-charged TiO$_2$ sample. This can be attributed to the presence of hydrogen ions in the TiO$_2$ crystal, where the defect levels lower the Fermi level of TiO$_2$ and decrease the Schottky barrier height at the interface and then result in a much higherμ_{eff} in Eq.4.1.

Vacuum annealing is another approach to induce dopants to TiO$_2$ for investigating the difference to hydrogen-charged TiO$_2$. To introduce oxygen vacancies in TiO$_2$, the bare crystals were thermally annealed at a 10^{-5} Pa and 700ºC for 2 hours. The flexoelectric measurement results suggest that there is no significant difference in the flexoelectric

coefficient between the annealed and pristine samples (Fig. 4.5). Compared to the significant increase of flexoelectricity for the hydrogen-charged TiO_2 crystal, it is suggested that hydrogen doping not only partially reduced the Ti^{4+} to Ti^{3+} but may also induce polarization in TiO_2 crystal structure due to the H^+ induced centrosymmetry breaking.
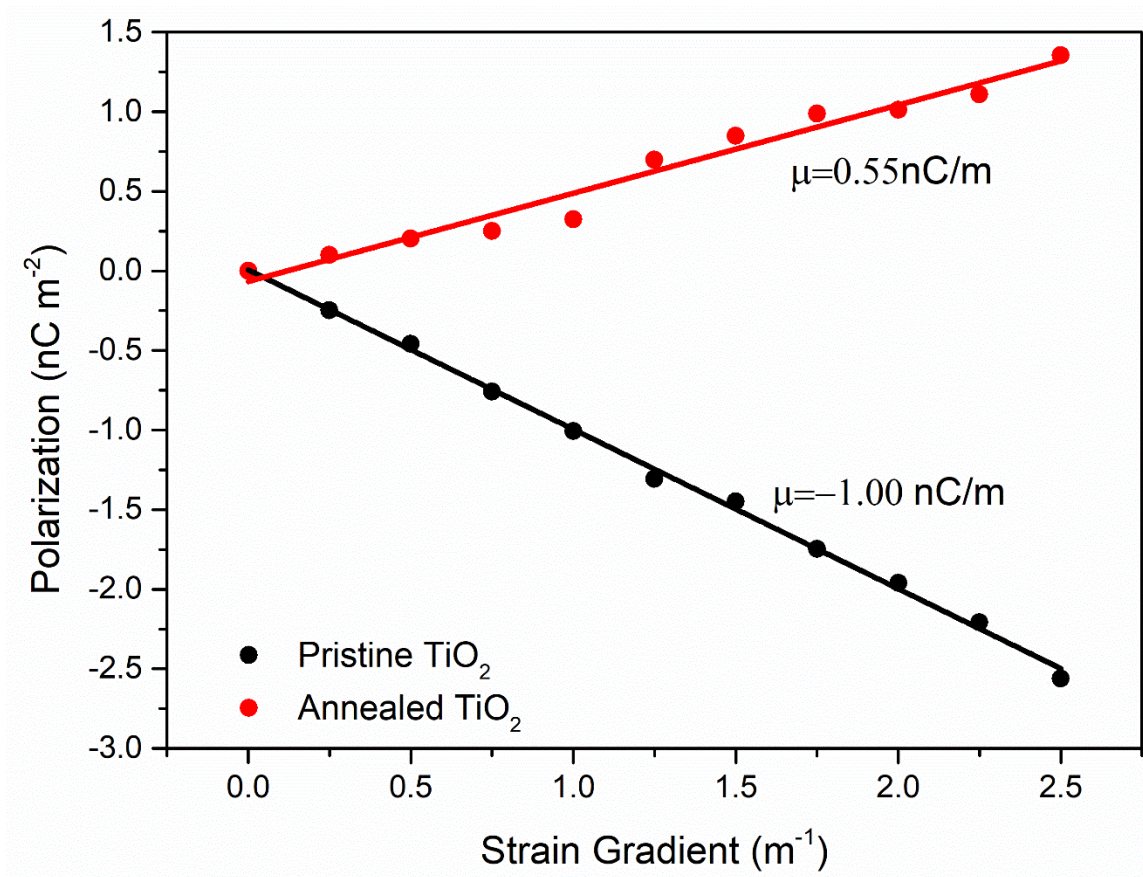

Figure 4.5 Effective flexoelectric effect of pristine and annealed TiO₂. There is no significant difference in flexoelectric coefficients between pristine TiO₂ and annealed TiO₂, but the sign is reversed.

We worked with Prof. Hong on the DFT calculation part. Based on the Modified model, **a** is 4.64 Å (pristine 4.66 Å), **b** is 4.71 Å (pristine 4.66 Å), and **c** is 2.97Å (pristine 4.66 Å) for hydrogen-charged TiO_2. After hydrogen charging, the lattice is distorted, and its unit cell expands in **a** direction and shrinks in the **b** and **c** direction. Weak O-H bonding is suggested to be formed, resulting in an expanded lattice. The structure of crystal lattice changes from cubic (Fig. 4.6a) to tetragonal (Fig. 4.6b). This result suggests that hydrogen doping in TiO_2 crystal and formation of O-H bonding may induce an electric polarization in its unit cells, and therefore, a very large flexoelectric effect can be achieved. The bonding angle of O-H may also be easily changed under strain gradient, giving rise to large flexoelectricity. A more detailed study in modeling needs to be carried out to understand the physics behind this interesting result.
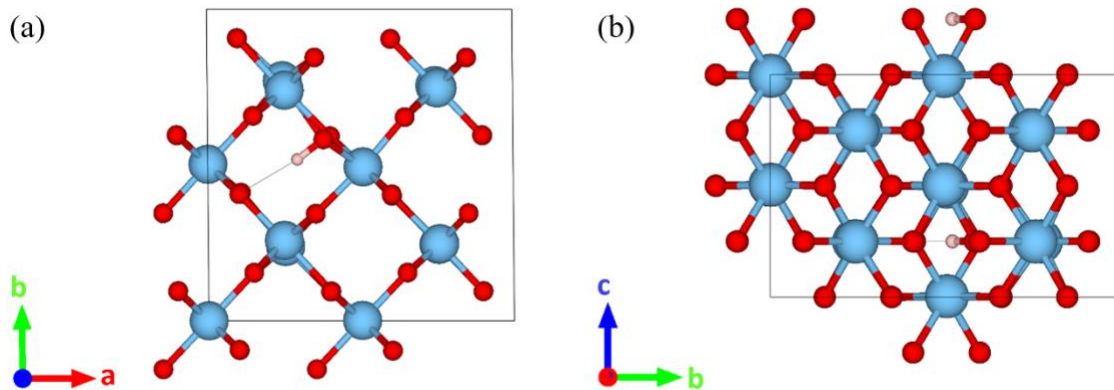
Figure 4.6 Schematic diagram of Modified model by hydrogen charging.

4.3 Summary

In conclusion, the doping effect has been studied in TiO_2 crystals. It is found that by introducing hydrogen in TiO_2, the effective flexoelectric coefficient can be enhanced by more than two orders of magnitude, compared with the stoichiometry ones. These results help us to understand the mechanism of flexoelectricity and may provide hints of more correlation effects on enhanced flexoelectricity. The increased flexoelectric coefficient may also have application prospects like energy harvesters, and accelerometers.

Chapter V

Conclusions and Suggestions for Future Work

5.1 Conclusions

By taking STO and TiO_2 single crystals as a standard sample, in this thesis work, the intrinsic and non-intrinsic flexoelectric effects are studied. The results demonstrate enhanced flexoelectricity through photo-flexoelectric effect and doping-induced carrier increase as well as electric polarization. The results of this thesis describe a new phenomenon at the STO and TiO_2 bulk crystal and provide new techniques to improve the flexoelectricity to influence both intrinsic and extrinsic properties of materials. The following conclusions are reached:

(1) The photo-flexoelectric effect has been demonstrated in STO crystals including pristine, vacuum annealed, hydrogen, and Nb-doped samples. It is found that by introducing UV light stimulations and oxygen vacancies, as well hydrogen and Nb doping in STO, the effective flexoelectric coefficient can be enhanced by more than two orders of magnitude, compared with the pristine sample.

(2) Formation of interfacial Schottky junction and the modulation of the junction height and thickness by oxygen vacancies and photo-generated current is attributed to be

responsible for the enhanced flexoelectricity. Doping-induced energy levels within the bandgap are also light absorption centers and the generated charge carriers will be driven by the flexoelectric field, giving rise to the enhanced flexoelectricity.

(3) Hydrogen doping into TiO_2 has been achieved by electrochemical reaction. Hydrogen doping in TiO_2 has been demonstrated to result in more significantly enhanced flexoelectricity. Hydrogen-induced electric polarization in the unit cell as well as the degradation of Ti^{4+} is attributed to be responsible for the enhanced flexoelectricity.

5.2 Suggestions for future works

There is still a lot of work that needs to be done to further study the mechanism of enhanced flexoelectricity in different systems such as semiconductors and thin films etc. During the experiment, I also found that the pressure applied to the sample surface will affect the flexoelectric coefficient. Next, we hope to be able to apply incremental pressure on the sample by using bending models of different depths. In this way, it is a new method to increase flexoelectricity and broaden the applications. Many potential applications with enhanced flexoelectricity need to be demonstrated in the future, for example, photo-flexoelectric enhanced catalysis, photo-sensing, solar cells, vibration sensing devices.

References

[1] Xiang Yan, Wenbin Huang, Seol Ryung Kwon, Shaorui Yang, Xiaoning Jiang, and Fuh-Gwo Yuan, Smart Materials and Structures **22** (8), 085016 (2013).

[2] Lee, D.; Yoon, A.; Jang, S. Y.; Yoon, J. G.; Chung, J. S.; Kim, M.; Scott, J. F.; Noh, T. W., *Physical Review Letters* **2011**, 107 (5), 057602.

[3] Wenhui Ma and L Eric Cross, Applied Physics Letters **86** (7), 072905 (2005).

[4] Liping Liu, Journal of the Mechanics and Physics of Solids **63**, 451 (2014).

[5] Longfei Wang, Shuhai Liu, Xiaolong Feng, Chunli Zhang, Laipan Zhu, Junyi Zhai, Yong Qin, and Zhong Lin Wang, Nature Nanotechnology **15** (8), 661 (2020).

[6] Pavlo Zubko, Gustau Catalan, and Alexander K Tagantsev, Annual Review of Materials Research **43,** 387 (2013).

[7] Fan Zhang, Peng Lv, Yiteng Zhang, Shujin Huang, Chi-Man Wong, Hei-Man Yau, Xinxin Chen, Zheng Wen, Xiaoning Jiang, and Changgan Zeng, Physical review letters **122** (25), 257601 (2019).

[8] A. E. Clark, J. P. Teter, and O. D. McMasters, Journal of Applied Physics **63**, 3910 (1988).

[9] P. Harris, Journal of Applied Physics **36**, 739 (1965).

[10] A. K. Tagantsev, Phase Transitions **35**, 119 (1991).

[11] A. Tagantsev, Soviet Physics Uspekhi **30**, 588 (1987).

[12] S. V. Kalinin and A. N. Morozovska, Nat. Nanotechnol. 10, 916 (2015)

[13] Ming-Min Yang, Dong Jik Kim, and Marin Alexe, Science **360** (6391), 904 (2018).

[14] Haiyang Zou, Chunli Zhang, Hao Xue, Zhiyi Wu, and Zhong Lin Wang, ACS Nano 2019 13 (11), 12259-12267

[15] L Eric Cross, Journal of Materials Science **41** (1), 53 (2006).

[16] Amir Abdollahi, Fabián Vásquez-Sancho, and Gustau Catalan, Physical review letters **121** (20), 205502 (2018).

[17] Xiaotong Zhang, Qi Pan, Dongxia Tian, Wanfeng Zhou, Pan Chen, Haifeng Zhang, and Baojin Chu, Physical review letters **121** (5), 057602 (2018).

[18] Xiaoning Jiang, Wenbin Huang, and Shujun Zhang, Nano Energy **2** (6), 1079 (2013).

[19] Shujin Huang, Lu Qi, Wenbin Huang, Longlong Shu, Shenjie Zhou, and Xiaoning Jiang, Journal of Advanced Dielectrics **8** (02), 1830002 (2018).

[20] Bo Wang, Yijia Gu, Shujun Zhang, and Long-Qing Chen, Progress in Materials Science **106**, 100570 (2019).

[21] Wenbin Huang, Seol-Ryung Kwon, Shujun Zhang, Fuh-Gwo Yuan, and Xiaoning Jiang, Journal of Intelligent Material Systems and Structures **25** (3), 271 (2014).

[22] Haidong Lu, C-W Bark, D Esque De Los Ojos, J Alcala, Chang-Beom Eom, G Catalan, and Alexei Gruverman, Science **336** (6077), 59 (2012).

[23] Gustau Catalan, AHGV Lubk, AHG Vlooswijk, E Snoeck, C Magen, A Janssens, Gijsbert Rispens, G Rijnders, Dave HA Blank, and Beatriz Noheda, Nature materials **10** (12), 963 (2011).

[24] Sergei V Kalinin and Anna N Morozovska, Nature nanotechnology **10** (11), 916 (2015).

[25] Xiang Yan, Wenbin Huang, Seol Ryung Kwon, Shaorui Yang, Xiaoning Jiang, and Fuh-Gwo Yuan, Smart Materials and Structures **22** (8), 085016 (2013).

[26] Alexander K Tagantsev and Alexander S Yurkov, Journal of Applied Physics **112** (4), 044103 (2012).

[27] Eugene A Eliseev, Anna N Morozovska, Maya D Glinchuk, and R Blinc, Physical Review B **79** (16), 165433 (2009).

[28] Umesh Kumar Bhaskar, Nirupam Banerjee, Amir Abdollahi, Zhe Wang, Darrell G Schlom, Guus Rijnders, and Gustau Catalan, Nature nanotechnology **11** (3), 263 (2016).

[29] Xin Wen, Dongfan Li, Kai Tan, Qian Deng, and Shengping Shen, Physical review letters **122** (14), 148001 (2019).

[30] Saikat Das, Bo Wang, Tula R Paudel, Sung Min Park, Evgeny Y Tsymbal, Long-Qing Chen, Daesu Lee, and Tae Won Noh, Nature communications **10** (1), 1 (2019).

[31] Jackeline Narvaez, Fabian Vasquez-Sancho, and Gustau Catalan, Nature **538** (7624), 219 (2016).

[32] Zhong Lin Wang, Advanced Materials **19** (6), 889 (2007).

[33] Wenzhuo Wu and Zhong Lin Wang, Nature Reviews Materials **1** (7), 1 (2016).

[34] Yan Zhang, Ying Liu, and Zhong Lin Wang, Advanced Materials **23** (27), 3004 (2011).

[35] Zhong Lin Wang and Wenzhuo Wu, National Science Review **1** (1), 62 (2014).

[36] VG Zalesskii and ED Rumyantseva, Physics of the Solid State **56** (7), 1352 (2014).

[37] G. Peng, S. Yang, R. Ishikawa, L. Ning, and Y. Ikuhara, Physical Review Letters **120** (2018).

[38] K. D. Breneman, W. E. Brownell, and R. D. Rabbitt, PLOS ONE **4**, e5201 (2009).

[39] F. Vasquez-Sancho, A. Abdollahi, D. Damjanovic, and G. Catalan, Advanced Materials **30**, 1705316 (2018).

[40] C. A. Mizzi, A. Y. W. Lin, and L. D. Marks, Physical Review Letters **123**, 116103 (2019).

[41] Toda, M. & Thompson, M. L. IEEE Sens. J. 6, 1170–1177 (2006).

[42] Davis, D. & Patronis, E. Sound System Engineering 3rd edn (Focal Press, 2006).

[43] Lang, C., Fang, J., Shao, H. Xin Ding & Tong Lin. Nat Commun 7, 11108 (2016).

[44] G.V. Békésy, Science 123 (3201) (1956) 779–783

[45] G.V. Békésy, J. Acoust. Soc. Am. 35 (4) (1963) 588–601.

[46] Gong, S. et al. Advanced Functional Materials, 1910717 (2020).

[47] Shintaku, H. et al. Sensors and Actuators A: Physical 158, 183-192 (2010).

[48] KF Wang and BL Wang, Energy **149**, 597 (2018).

[49] Shuwen Zhang, Kaiyuan Liu, Minglong Xu, and Shengping Shen, Applied Physics Letters **111** (8), 082904 (2017).

[50] X Yan, WB Huang, SR Kwon, SR Yang, XN Jiang, and FG Yuan, presented at the Sensors and Smart Structures Technologies for Civil, Mechanical, and Aerospace Systems

2013, 2013 (unpublished).

[51] R. Sarlo, D. Leo, Proceedings of the ASME 2015 Conference

[52] Harris P. 1965. *J. Appl. Phys.* 36(3):739–41

[53] W, H. Baur, Acta Cryst. 9, 515 (1956)

[54] Christoph J Raub, Plat Surf Finish **80** (9), 30 (1993).

[55] Jiang Li Cao, Long Tu Li, Yong Li Wang, Jian Qiang Zhao, and Zhi Lun Gui, Materials research bulletin **36** (12), 2103 (2001).

[56] Wan Ping Chen, Yu Wang, Xiao Xing Wang, Jie Wang, and Helen Lai Wah Chan, Materials chemistry and physics **82** (3), 520 (2003).

[57] Longlong Shu, Shanming Ke, Linfeng Fei, Wenbin Huang, Zhiguo Wang, Jinhui Gong, Xiaoning, Jiang, Li Wang, Fei Li, and Shuijin Lei, Nature materials, **19**, 605 (2020).

[58] Rui Guo, Lu You, Weinan Lin, Amr Abdelsamie, Xinyu Shu, Guowei Zhou, Shaohai Chen, Liang Liu, Xiaobing Yan, and Junling Wang, Nature communications **11** (1), 2571 (2020).

[59] Dennis V Christensen, Merlin von Soosten, Felix Trier, Thomas S Jespersen, Anders Smith, Yunzhong Chen, and Nini Pryds, Advanced Electronic Materials **3** (8), 1700026 (2017).

[60] Jackeline Narvaez, Fabian Vasquez-Sancho, and Gustau Catalan, Nature **538** (7624), 219 (2016).

[61] Akira Ohtomo and Harold Y Hwang, Journal of Applied Physics **102** (8), 083704 (2007)

[62] Marianne C Tarun, Farida A Selim, and Matthew D McCluskey, Physical Review Letters **111** (18), 187403 (2013).

[63] Shiu-Ming Huang, Shih-Jhe Huang, You-Jhih Yan, Shih-Hsun Yu, Mitch Chou, Hung-Wei Yang, Yu-Shin Chang, and Ruei-San Chen, RSC advances **7** (62), 39057 (2017).

[64] Changyong Lan, Chun Li, Yi Yin, Huayang Guo, and Shuai Wang, Journal of Materials Chemistry C **3** (31), 8074 (2015).

[65] You-Rong Tao, Xing-Cai Wu, and Wei-Wei Xiong, Small **10** (23), 4905 (2014).

[66] Xing Xie, So-Ying Kwok, Zhenzhen Lu, Yankuan Liu, Yulin Cao, Linbao Luo, Juan Antonio Zapien, Igor Bello, Chun-Sing Lee, and Shuit-Tong Lee, Nanoscale **4** (9), 2914 (2012).

[67] Benjamin J Hansen, Nikolai Kouklin, Ganhua Lu, I-Kuan Lin, Junhong Chen, and Xin Zhang, The Journal of Physical Chemistry C **114** (6), 2440 (2010).

[68] Xuming Xie and Guozhen Shen, Nanoscale **7** (11), 5046 (2015).

[69] Mehrdad Shaygan, Keivan Davami, Nazli Kheirabi, Changi Ki Baek, Gianaurelio Cuniberti, M Meyyappan, and Jeong-Soo Lee, Physical Chemistry Chemical Physics **16** (41), 22687 (2014).

[70] Reui-San Chen, Hsin-Yi Chen, Chien-Yao Lu, Kuei-Hsien Chen, Chin-Pei Chen, Li-Chyong Chen, and Ying-Jay Yang, Applied Physics Letters **91** (22), 223106 (2007).

[71] Violet M Poole, Caleb D Corolewski, and Matthew D McCluskey, AIP Advances **5** (12), 127217 (2015).

[72] Leonardo Triggiani, Ana B Muñoz-García, Angela Agostiano, and Michele Pavone, Physical Chemistry Chemical Physics **18** (41), 28951 (2016).

[73] Tomohito Tanaka, Katsuyuki Matsunaga, Yuichi Ikuhara, and Takahisa Yamamoto, Physical Review B **68** (20), 205213 (2003).

[74] Xinqiang Pan, Yao Shuai, Chuangui Wu, Wenbo Luo, Xiangyu Sun, Huizhong Zeng, Xiaoyuan Bai, Chaoguan Gong, Ke Jian, and Lu Zhang, Applied Physics A **123** (9), 1 (2017).

[75] Doo Seok Jeong, Herbert Schroeder, Uwe Breuer, and Rainer Waser, Journal of applied physics **104** (12), 123716 (2008).

[76] Xiaoning Jiang, Wenbin Huang, and Shujun Zhang, Nano Energy **2** (6), 1079 (2013).

[77] Shujin Huang, Lu Qi, Wenbin Huang, Longlong Shu, Shenjie Zhou, and Xiaoning Jiang, Journal of Advanced Dielectrics **8** (02), 1830002 (2018).

[78] Bo Wang, Yijia Gu, Shujun Zhang, and Long-Qing Chen, Progress in Materials Science **106**, 100570 (2019).

[79] Wenbin Huang, Seol-Ryung Kwon, Shujun Zhang, Fuh-Gwo Yuan, and Xiaoning Jiang, Journal of Intelligent Material Systems and Structures **25** (3), 271 (2014).

[80] SR Aggarwal, CW Perusse, R Ramesh Tipton, Drew HD, DB T Venkatesan, and VB Romero, Appl. Phys. Lett **73** (14), 1973 (1998).

[81] N Poonawala, VP Dravid, O Auciello, J Im, and AR Krauss, Journal of Applied Physics **87** (5), 2227 (2000).

[82] Joon-Hyung Ahn, Paul C McIntyre, Laura Wills Mirkarimi, Stephen R Gilbert, Jun Amano, and Michelle Schulberg, Applied Physics Letters **77** (9), 1378 (2000).

[83] J.M. Herbert, The properties of dielectrics, in D.S. Campbell (Ed.), Ceramic Dielectrics and Capacitors, Gordon and Breach, New York, 1985, pp. 57–62.

[84] Chen, X. B., Liu, L., Yu, P. Y. & Mao, S. S. *Science* **331,** 746–750 (2011).

[85] Wang, G. *et al. Nano Lett.* **11,** 3026–3033 (2011).

[86] Herklotz, F., Lavrov, E. V. & Weber, J. Infrared absorption of the hydrogen donor in rutile TiO_2. *Phys. Rev. B* **83,** 235202 (2011).

[87] Kilic, C. & Zunger, A. n-type doping of oxides by hydrogen. *Appl. Phys. Lett.* **81,** 73–75 (2002).

[88] Liu, L., Yu, P. Y., Chen, X. B., Mao, S. S. & Shen, D. Z. *Phys. Rev. Lett*. **111,** 065505 (2013).

[89] Naldoni, A. *et al. J. Am. Chem. Soc.* **134,** 7600–7603 (2012).

[90] Wanping Chen, Longtu Li, Yu Wang, and Zhilun Gui, Journal of materials research **13** (5), 1110 (1998).

[91] J. Im, O. Auciello, A. R. Krauss, D. M. Gruen, R. P. H. Chang, S. H. Kim, and A. I. Kingon, Appl. Phys. Lett. 78, 1162 ~1999!

[92] WP Chen, Yu Wang, JY Dai, SG Lu, XX Wang, PF Lee, Helen LW Chan, and CL Choy, Applied physics letters **84** (1), 103 (2004).

[93] Yangshi Jin, Fan Zhang, Kai Zhou, Chun Hung Suen, XY Zhou, and Ji-Yan Dai, Applied Physics Letters **118** (16), 164101 (2021).

[94] Doo Seok Jeong, Herbert Schroeder, Uwe Breuer, and Rainer Waser, Journal of applied physics **104** (12), 123716 (2008).

[95] Pascal A Baldi, Marc P De Micheli, Kasem El Hadi, Salim Nouh, Alfonso C Cino, P Aschieri, and Daniel B Ostrowsky, Optical Engineering **37** (4), 1193 (1998).

[96] Jackeline Narvaez, Fabian Vasquez-Sancho, and Gustau Catalan, Nature **538** (7624), 219 (2016).